International Journal of Bifurcation and Chaos, Vol. 14, No. 9 (2004) 3179–3204

BIFURCATIONS AND CHAOS IN TWO-CELL CELLULAR NEURAL NETWORKS WITH PERIODIC INPUTS

SONG-SUN LIN*
Department of Applied Mathematics, National Chiao-Tung University, Hsin-Chu 30050, Taiwan

WEN-WEI LIN†
Department of Mathematics, National Tsing-Hua University, Hsin-Chu 30050, Taiwan

TING-HUI YANG*
Department of Applied Mathematics, National Chiao-Tung University, Hsin-Chu 30050, Taiwan

Received May 30, 2003; Revised September 8, 2003

This study investigates bifurcations and chaos in two-cell Cellular Neural Networks (CNN) with periodic inputs. Without the inputs, the time periodic solutions are obtained for template $A = [r, p, s]$ with $p > 1$, $r > p - 1$ and $-s > p - 1$. The number of periodic solutions can be proven to be no more than two in exterior regions. The input is $b \sin 2\pi t/T$ with period $T > 0$ and amplitude $b > 0$. The typical trajectories $\Gamma(b, T, A)$ and their ω-limit set $\omega(b, T, A)$ vary with b, T and A are also considered. The asymptotic limit cycles $\Lambda_\infty(T, A)$ with period T of $\Gamma(b, T, A)$ are obtained as $b \to \infty$. When $T_0 \le T_0^*$ (given in (67)), Λ_∞ and $-\Lambda_\infty$ can be separated. The onset of chaos can be induced by crises of $\omega(b, T, A)$ and $-\omega(b, T, A)$ for suitable T and b. The ratio $\mathcal{A}(b) = |a_T(b)|/|a_1(b)|$, of largest amplitude $a_1(b)$ except for T-mode and amplitude of the T-mode of the Fast Fourier Transform (FFT) of $\Gamma(b, T, A)$, can be used to compare the strength of sustained periodic cycle $\Lambda_0(A)$ and the inputs. When $\mathcal{A}(b) \ll 1$, $\Lambda_0(A)$ dominates and the attractor $\omega(b, T, A)$ is either a quasi-periodic or a periodic. Moreover, the range b of the window of periodic cycles constitutes a devil's staircase. When $\mathcal{A}(b) \sim 1$, finitely many chaotic regions and window regions exist and interweave with each other. In each window, the basic periodic cycle can be identified. A sequence of period-doubling is observed to the left of the basic periodic cycle and a quasi-periodic region is observed to the right of it. For large b, the input dominates, $\omega(b, T, A)$ becomes simpler, from quasi-periodic to periodic as b increases.

Keywords: Cellular neural networks; CNN; chaos; crises; fractal; Lady's shoe; Lyapunov exponent.

*Work partially supported by the NSC under Grant No. 89-2115-M-008-029, the Lee and MTI Center for Networking Research and the National Center for Theoretical Sciences Mathematics Division, R.O.C.
†Work partially supported by the NSC under Grant No. 91-2115-M-007-006 and the National Center for Theoretical Sciences Mathematics Division, R.O.C.

1. Introduction

Following the introduction by Chua and Yang [1988a, 1988b], Cellular Neural Networks (CNN) have been extensively studied, see [Chua, 1998; Manganaro *et al.*, 1999; Chua & Roska, 2002] and references therein. Two of their applications are in image processing and pattern recognition. An important class related to applications are steady-state solutions including mosaic solutions and defection solutions [Chua, 1998; Manganaro *et al.*, 1999; Hsu *et al.*, 2000; Juang & Lin, 1997, 2000]. The complexity of steady-state solutions have recently been extensively studied [Ban *et al.*, 2001a; Ban *et al.*, 2002; Ban *et al.*, 2001b; Hsu *et al.*, 2000; Hsu & Lin, 2001; Hsu & Yang, 2002; Juang & Lin, 2000; Juang & Lin, 1997; Lin & Shih, 1999; Lin & Yang, 2000; Lin & Yang, 2002]. Furthermore, without the input terms, the theory of complete stability for CNN with symmetric feedback template have been proven in [Lin & Shih, 1999; Shih, 2001; Wu & Chua, 1997]. However, when the feedback template is antisymmetric, the time dependent periodic solutions have been obtained by Thiran [1997].

Zou and Nossek [1991] discovered a chaotic attractor in a two-cell CNN with an antisymmetric feedback template and a periodic input. Motivated by [Zou & Nossek, 1991], this study addresses the bifurcations and chaos of a two-cell CNN with periodic inputs in a general situation. Indeed,

$$\begin{cases} \dot{x_1} = -x_1 + py_1 + sy_2 + bu(t)\,, \\ \dot{x_2} = -x_2 + ry_1 + py_2\,, \end{cases} \tag{1}$$

is studied with the output function

$$y = f(x) = \frac{1}{2}(|x+1| - |x-1|)\,, \tag{2}$$

where the feedback template $A = [r,\, p,\, s]$, satisfies

$$p > 1, \quad p - 1 < r \quad \text{and} \quad p - 1 < -s\,. \tag{3}$$

The input function (or forcing function), as in [Zou & Nossek, 1991], is

$$u(t) = \sin\frac{2\pi}{T}t\,, \tag{4}$$

with period $T > 0$ and amplitude $b > 0$.

The bifurcations of (1) involve five parameters: r, p, s, T and b. The strategy employed is to begin with $b = 0$ and a template $A = [r,\, p,\, s]$, which satisfies (3). Without input, we are mainly concerned with the existence and uniqueness of limit cycle Λ_0. Λ_0 will interact with inputs $bu(t)$ and may cause complicated dynamics later. Then a suitable range of T and b is identified to ensure that (1) have chaotic attractors.

The template A governs the basic dynamics of (1). When $b = 0$ and (3) holds, (semi-)stable limit cycles always exist. Indeed, all trajectories, except the origin, will tend to the limit cycles as $t \to \infty$. Our numerical experience indicates that a unique limit cycle always applies. See Sec. 4 for details.

The impact of an input $bu(t)$ on its period T and amplitude b are studied. Consider (1) with initial conditions

$$x_1(0) = \xi_1 \quad \text{and} \quad x_2(0) = \xi_2\,. \tag{5}$$

The solution of (1) and (5) is denoted by

$$(x_1(t,\, \xi_1,\, \xi_2;\, b,\, T,\, A),\, x_2(t,\, \xi_1,\, \xi_2;\, b,\, T,\, A))\,. \tag{6}$$

The ω-limit set of (6) is denoted by

$$\omega(\xi_1,\, \xi_2;\, b,\, T,\, A)\,, \tag{7}$$

and the nonwandering set of (1) is denoted by

$$\Omega(b,\, T,\, A) = \overline{\bigcup_{(\xi_1,\, \xi_2)\in\mathbb{R}^2} \omega(\xi_1,\, \xi_2;\, b,\, T,\, A)}\,. \tag{8}$$

Since the input is T-periodic, for a fixed parameter A, T and b, a two-dimensional Poincaré map of (1) can be defined as

$$F(\xi_1,\, \xi_2) = (x_1(T,\, \xi_1,\, \xi_2),\, x_2(T,\, \xi_1,\, \xi_2))\,. \tag{9}$$

Now, the study of the bifurcations problem of (1) is equivalent to the study of how $\Omega(b,\, T,\, A)$ changes when b, T and A vary. To simplify the problem, rather than studying $\Omega(b,\, T,\, A)$, this paper is concerned mainly with how "typical" trajectories vary with b, T and A. In particular, when $b > 0$, the trajectory $\Gamma_b \equiv \Gamma(b,\, T,\, A)$ of (6) and ω-limit set $\omega_b \equiv \omega(b,\, T,\, A)$ of (7) with the initial condition at the origin $O = (0,\, 0)$ are considered. The ω-limit set of the Poincaré map is denoted by $\hat{\omega}(b,\, T,\, A)$. To show $\Omega(b,\, T,\, A)$ is a chaotic attractor, the following conditions must be proven to hold.

(i) $\Gamma(b,\, T,\, A)$ has a positive Lyapunov exponent,
(ii) $\hat{\omega}(b,\, T,\, A)$ is fractal,
(iii) FFT (Fast Fourier Transform) of $\Gamma(b,\, T,\, A)$ has a broad-band.

An effective approach of studying effects of the input period T is to examine the asymptotic limit cycle $\Lambda_\infty(T,\, A)$ by letting $b \to \infty$. When $T \le T_0^*$ (defined in (67)) then Λ_∞ and $-\Lambda_\infty$ can be separated. Therefore $\omega(b,\, T,\, A)$ and $-\omega(b,\, T,\, A)$ are separated for large b but collide when b is small. If b becomes even smaller, a chaotic attractor may

develop. Indeed, the onset of chaos induced by crises of $\omega(b, T, A)$ and $-\omega(b, T, A)$ were observed for suitable T and b. For details, please see Fig. 13 and Sec. 6.

After an interesting range of T is identified, the effect of b can be examined. Intuitively, the unperturbed limit cycle will dominate when b is small. Indeed, FFT of $\Gamma(b, T, A)$ is considered when $b > 0$ and is relatively small. Let T_b be the period with the largest amplitude $a_1(b)$ of FFT on $x_1(t, 0, 0; b, T, A)$ except for T-mode, and $a_T = a_T(b, T, A)$ be the amplitude of the period T mode. The ratio

$$\mathcal{A}(b) \equiv \left|\frac{a_T(b)}{a_1(b)}\right| \tag{10}$$

represents the relative strength of the T-mode with respect to the T_b-mode as b varies. Equation (1) is called T_b dominant if $\mathcal{A}(b) \ll 1$, the T_b and T modes are comparable if $\mathcal{A}(b) \simeq 1$ but T is dominant if $\mathcal{A}(b) \gg 1$.

When T_b is dominant, ω_b is found to be either quasi-periodic or periodic. The periodic windows typically form a devil's staircase when $b \in (b_*, b_0^*)$, where $0 < b_* < b_0^*$ depends on A and T. For example, Figs. 3 and 11 present the ZN-case in [Zou & Nossek, 1991], that is $A = [1.2, 2, -1.2]$ and $T = 4$.

When T_b and T modes are comparable, the Lyapunov exponents of $\Gamma(b, T, A)$ and ω-limit set $\hat{\omega}(b, T, A)$ of Poincaré map are computed. In many interesting cases, including the ZN-case, finitely many chaotic and window regions interweave with each other. In chaotic regions, the largest Lyapunov exponent is positive and $\hat{\omega}(b, T, A)$ is fractal, as in Fig. 15. $\hat{\omega}(b, T, A)$ looks like a lady's shoe as in the ZN-case and contains a horseshoe as in asymmetric templates case, as shown in Figs. 20 and 23. In each window, the basic periodic cycle can be identified, i.e. the periodic cycle with the minimum period. In the window, a sequence of period-doubling is observed to the left of the basic periodic cycle. A quasi-periodic region is to the right of the basic periodic cycle.

For b large, the T-mode dominates, the attractors $\omega(b, T, A)$ gets simpler, from quasi-periodic to periodic as b increases. See Sec. 6.

The rest of this paper is organized as follows. Section 2 introduces some properties of solutions of (1) which will be useful later. Section 3 introduces a program for studying bifurcations and chaos since many parameters are involved. The limit cycle of (1) is first studied without input. Then, methods are developed to identify possible ranges of T and b to ensure the occurrence of interesting bifurcation and the existence of chaotic attractors. Section 4 addresses the existence and uniqueness of the limit cycle of (1) when $b = 0$ and (3) holds. Section 5 uses the FFT of $\Gamma(b, T, A)$ to study the bifurcations when b is relative small, i.e. when T_b dominates. Section 6 studies the asymptotic limit cycle when $b \to \infty$. Section 7 studies chaos when T_b and T modes are comparable. Section 8 introduces our numerical methods. Section 9 briefly discusses results and offers suggestions for future study.

2. Preliminaries

This section provides some preliminary results of (1). Given an initial condition

$$(x_1(0), x_2(0)) = (\xi_1, \xi_2)\,, \tag{11}$$

the solution of (1) with (11) is denoted by $(x_1(t; \xi_1, \xi_2), x_2(t; \xi_1, \xi_2))$. We first state some symmetric properties of the solutions of (1).

Theorem 2.1.

(i) *If $(x_1(t), x_2(t))$ is a solution of (1), then*

$$\left(-x_1\left(t + \frac{T}{2}\right), -x_2\left(t + \frac{T}{2}\right)\right) \tag{12}$$

is also a solution of (1). In particular, if $b = 0$, then $(-x_1(t), -x_2(t))$ is also a solution.

(ii) *If $b \neq 0$ and $(x_1(t), x_2(t))$ is a periodic solution of (1), then its period is mT for some positive integer m.*

(iii) *When $b = 0$ and A is antisymmetric, i.e. $s = -r$, if $(x_1(t), x_2(t))$ is a solution of (1), then*

$$(x_2(t), -x_1(t)) \tag{13}$$

is also a solution.

Proof

(i) Since

$$f(-x) = -f(x) \quad \text{and} \quad u\left(t + \frac{T}{2}\right) = -u(t)\,, \tag{14}$$

the function given in (12) is clearly also a solution.

(ii) Assume that $(x_1(t), x_2(t))$ is a periodic solution with period $\tilde{T} > 0$; then $x_1(t + \tilde{T}) = x_1(t)$ and $x_2(t + \tilde{T}) = x_2(t)$ imply $\sin(2\pi/T)(t + \tilde{T}) = \sin(2\pi/T)t$ for all t. Hence, $\tilde{T} = mT$ for some positive integer m.

(iii) When $b = 0$ and $s = -r$, let $(v_1(t), v_2(t)) = (x_2(t), -x_1(t))$. Then, (v_1, v_2) satisfies $\dot{v_1} = -v_1 + pw_1 + sw_2$ and $\dot{v_2} = -v_2 + rw_1 + pw_2$, where $w_j = f(v_j)$ and $j = 1, 2$. Hence, (13) is also a solution. The proof is complete.

■

A set $S \subseteq \mathbb{R}^2$ is called symmetric with respect to $O = (0, 0)$, if

$$-S = S\,, \tag{15}$$

where $-S = \{(-x_1, -x_2) \in \mathbb{R}^2 | (x_1, x_2) \in S\}$. Otherwise, S is called asymmetric. In particular, a trajectory $(x_1(t; \xi_1, \xi_2), x_2(t; \xi_2, \xi_2))$ of (1) is called symmetric if the set $\Gamma(\xi_1, \xi_2) = \{(x_1(t), x_2(t)) | t \in \mathbb{R}^1$ and $(x_1(0), x_2(0)) = (\xi_1, \xi_2)\}$ is symmetric.

The isoclines are useful in studying (1). The x_2-isocline $\dot{x_2} = 0$ is independent of time, i.e.

$$h(x_1, x_2) \equiv -x_2 + ry_1 + py_2 = 0\,. \tag{16}$$

The x_1-isoclines are time periodic with period T if $b > 0$, i.e.

$$g(x_1, x_2) \equiv -x_1 + py_1 + sy_2 = -b \sin \frac{2\pi}{T} t\,, \tag{17}$$

See Figs. 1 and 2.

Moving isoclines are first used to discuss the possible trajectories of (1). When (3) holds and $b = 0$, the origin $O = (0, 0)$ can be easily verified to be the only steady-state solution of (1). Furthermore, O is an unstable spiral with eigenvalues $\lambda = (p - 1) \pm i\sqrt{-rs}$. Figure 1 presents vector fields of (1) when $b = 0$. In this case, apart from O, all trajectories move counterclockwise around O and tend to a limit cycle. See Theorem 4.1 for details. However, when $b > 0$, the periodically moving x_1-isocline $g(x_1, x_2) = -bu(t)$ oscillates horizontally. At a given instant $\bar{t}$, $g(x_1, x_2) = -bu(\bar{t})$ may intersect $h(x_1, x_2) = 0$ at point $(\bar{x}_1, \bar{x}_2)$. In that case, $(\bar{x}_1, \bar{x}_2)$ can be regarded as a "temporary or instantaneous steady-state". The trajectories which are near $(\bar{x}_1, \bar{x}_2)$ at time $\bar{t}$ may circle around $(\bar{x}_1, \bar{x}_2)$ thereafter. This basic mechanism can generate complicated trajectories as easily observed from the numerical simulations. See Figs. 2 and 13(d). The following sections will describe global trajectories.

With reference to a dynamical system of (1), the asymptotic behavior of trajectories as t tends to infinite is of most interest. Therefore, the ω-limit set for each trajectory must be studied. The ω-limit set of (1) and (11) is defined by

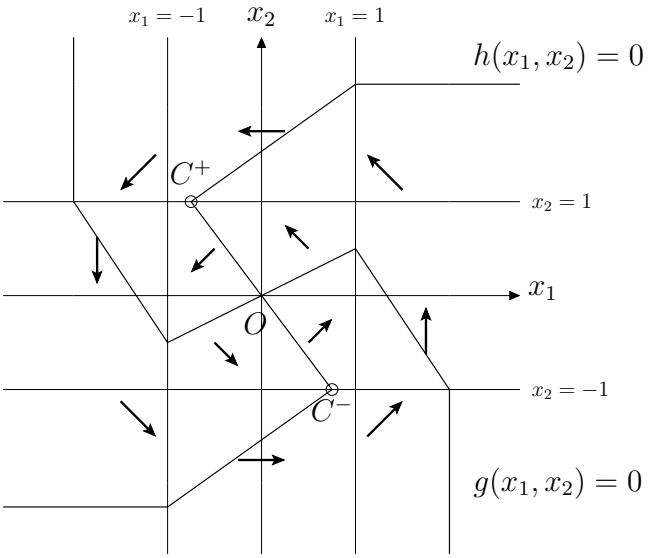

Fig. 1. Isoclines and vector fields of system (1) when $b = 0$.

$$\omega(\xi_1, \xi_2) = \{(\bar{x}_1, \bar{x}_2) \in \mathbb{R}^2 | \exists t_k \to \infty \text{ such that } x_i(t_k; \xi_1, \xi_2) \to \bar{x}_i,\ i = 1, 2\}\,. \tag{18}$$

The nonwandering set Ω of (1) is defined by

$$\Omega = \overline{\bigcup_{(\xi_1, \xi_2) \in \mathbb{R}^2} \omega(\xi_1, \xi_2)}\,. \tag{19}$$

Note that ω and Ω depend on the template A, T and b. To simplify the notation, the dependency is omitted if it does not cause confusion. However, $\omega_b(\xi_1, \xi_2)$ or $\omega(\xi_1, \xi_2; b)$ and Ω_b may be used to emphasize the dependency on b.

The main goal of this paper is to analyze $\omega_b(\xi_1, \xi_2)$ and Ω_b, and to study their bifurcations as parameters A, T and b vary. The following results can be derived from these isoclines and their associated vector fields in phase-plane as shown in Figs. 1 and 2.

Theorem 2.2. *Assume (3) and $b \geq 0$. The nonwandering set $\Omega_b \subseteq [-b - p + s, b + p - s] \times [-(p + r), p + r]$. Furthermore Ω_b is symmetric and attracts all trajectories as $t \to \infty$.*

Proof. For each $b \geq 0$, $\Omega_b \subseteq [-b - p + s, b + p - s] \times [-(p + r), p + r]$ can be easily verified from the associated vector fields in phase-plane. See Figs. 1 and 2. Clearly, Ω_b attracts all trajectories as $t \to \infty$.

By Theorem 2.1(i), Ω_b is symmetric. The proof is complete. ■

Remark 2.3. $b > 0$ may have an asymmetric periodic orbit Λ. In that case, an other asymmetric periodic orbit $-\Lambda$ exists, and $-\Lambda \cup \Lambda \subseteq \Omega_b$.

Since the inputs are periodic with period T, introducing a two-dimensional Poincaré map $F : \mathbb{R}^2 \to \mathbb{R}^2$ by

$$F(\xi_1, \xi_2) = (x_1(T; \xi_1, \xi_2), x_2(T; \xi_1, \xi_2)) \quad (20)$$

is natural. Clearly the periodic orbits of (1) with period mT are the periodic points of F with period m, and vice-versa.

The ω-limit set $\hat{\omega}_b(\xi_1, \xi_2)$ and the nonwandering set $\hat{\Omega}_b$ of Poincaré map F can also be studied. Indeed,

$$\hat{\omega}_b(\xi_1, \xi_2) = \{(\eta_1, \eta_2) \in \mathbb{R}^2 | \exists n_k \to \infty \text{ such that } F^{n_k}(\xi_1, \xi_2) \to (\eta_1, \eta_2) \text{ as } n_k \to \infty\}, \quad (21)$$

and

$$\hat{\Omega}_b = \bigcup_{(\xi_1, \xi_2) \in \mathbb{R}^2} \hat{\omega}_b(\xi_1, \xi_2). \quad (22)$$

Clearly, $\hat{\omega}_b(\xi_1, \xi_2) \subset \omega_b(\xi_1, \xi_2)$ and $\hat{\Omega}_b \subseteq \Omega_b$.

Now, the Lyapunov exponents of (1) can be studied using its Poincaré map F. Recall that the Lyapunov exponents of a smooth map F on $\mathbb{R}^m \to \mathbb{R}^m$ are defined as follows [Alligood *et al.*, 1997, pp. 194–195].

Definition 2.4. For a smooth map f on $\mathbb{R}^m$, let $J_n = Df^n(v_0)$, and for $k = 1, \ldots, m$, let R_k^n be the length of kth longest orthogonal axis of the ellipsoid $J_n U$ for an orbit with initial point v_0. Then R_k^n measures the contraction or expansion near the orbit of v_0 during the first n iterations. The kth Lyapunov exponent of v_0 is defined by $\alpha_k = \lim_{n\to\infty} \log((R_k^n)^{1/n})$, if the limit exist.

In this paper, the system (1) is called chaotic if the following conditions hold:

(i) the largest Lyapunov exponent of $\hat{\Omega}_b$ is positive,
(ii) $\hat{\Omega}_b$ is fractal,
(iii) some typical trajectories of (1) have broadbands under FFT.

Proving that a typical trajectory, say $\Gamma_b(0, 0)$ satisfies (i) and (ii) suffices to verify conditions (i) and (ii). The following sections present the relevant details.

3. Programs for Studying Bifurcations and Chaos

The rest of this paper addresses the bifurcations and chaos of (1) as the parameters $A = [r, p, s]$, T and b vary. The following programs are applied to study thoroughly a complex and interesting phenomenon over a range of parameters, since the problems involve five parameters.

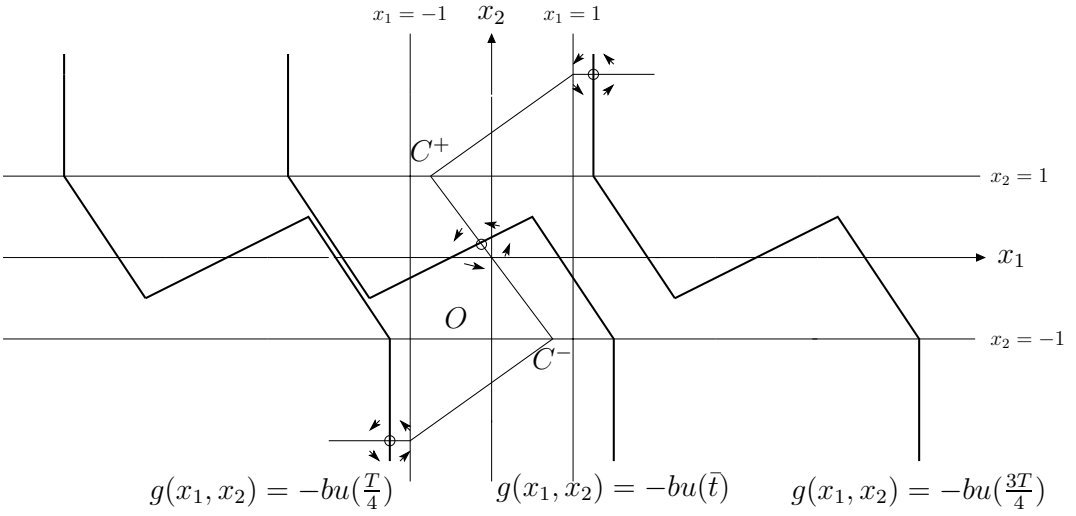

Fig. 2. Isoclines and vector fields for $b > 0$.

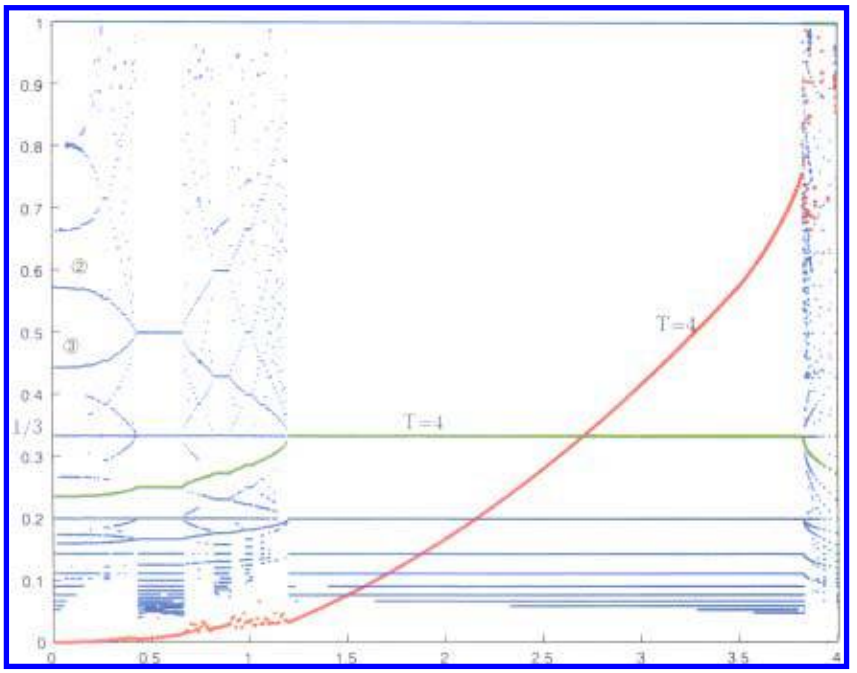

Fig. 3. FFT of the largest 20 modes for the ZN-case: $A = [1.2,\ 2,\ -1.2]$ and $T = 4$.

(I) Take $b = 0$ and study how the sustained limit cycles $\Lambda_0(A)$ vary with the template $A = [r,\ p,\ s]$. In particular, examine how the period $T_0(A)$ of $\Gamma_0(A)$ varies with A.

(II) Fix A. Find possible range of input periods T such that (1) exhibit chaotic behavior for suitable $b > 0$. In particular, try to find the relation between T and $T_0(A)$ such that (1) have complex trajectories for some $b > 0$.

(III) Fix A and T obtained in (I) and (II), try to identify critical numbers of b, say, $b_0^* < b_1^* < \cdots < b_k^*$, which represent various types of trajectories of (1) and may cause distinct bifurcations when b_j^* is crossed.

With reference to program (I), Sec. 4 discusses the existence and uniqueness of limit cycles. To explain how programs (II) and (III) are implemented, a series of numerical experiments with varying $b > 0$ are presented, as follows.

For fixed A and T, denote by Γ_b the forward-trajectory of (1) with the initial condition at the origin O, and ω_b the corresponding ω-limit set of Γ_b. Λ_0 is the (inner) limit cycle for $b = 0$ and is obtained from Theorem 4.1. Apply FFT to the x_1-component of Γ_b, i.e. $x_1(t;\ 0,\ 0)$, $t > 0$. Pick up the first N frequencies of these data, i.e. let $\{a_k e^{i\omega_k t}\}_{k=1}^N$ satisfy

$$|a_1| \geq |a_2| \geq \cdots \geq |a_N| \geq a_\omega\,, \tag{23}$$

for other frequency ω, where $a_k = a_k(b)$ and $\omega_k = \omega_k(b)$, denote

$$\tau_k(b) = \frac{2\pi}{\omega_k(b)}\,, \tag{24}$$

the period of the kth mode. For simplicity, denote

$$T_b = \tau_1(b)\,, \tag{25}$$

which corresponds to the largest amplitude except for T-mode. It is not difficult to verify

$$\lim_{b\to 0^+} T_b = T_0\,. \tag{26}$$

The normalized curves

$$R_k(b) = \frac{\tau_k(b)}{T_b} \tag{27}$$

of $\tau_k(b)$, and $1 \leq k \leq N$, are very useful for finding periodic orbits. To be more specific, in the ZN-case, $R_k(b)$ with $1 \leq k \leq 20$ and $b \in [0,\ 4]$ are as in Fig. 3.

Figure 3 can be explained as follows.

(1) The amplitude of the $T = 4$ mode (represented by a red thick line in Fig. 3) grows steadily as b increases in $(0,\ 3.826)$. It is comparable to T_b when b is close to 4, near the onset of chaos.

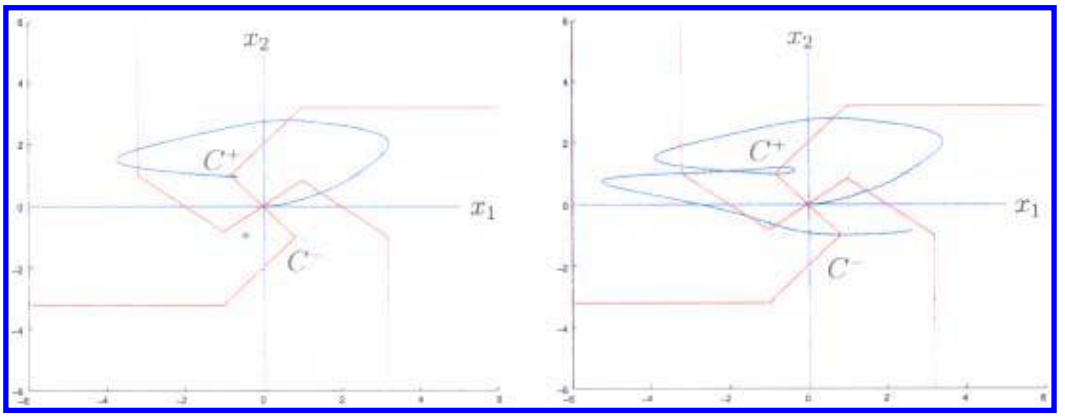

(a) $b_1^* = 3.98$ (b) $b_2^* = 4.284$

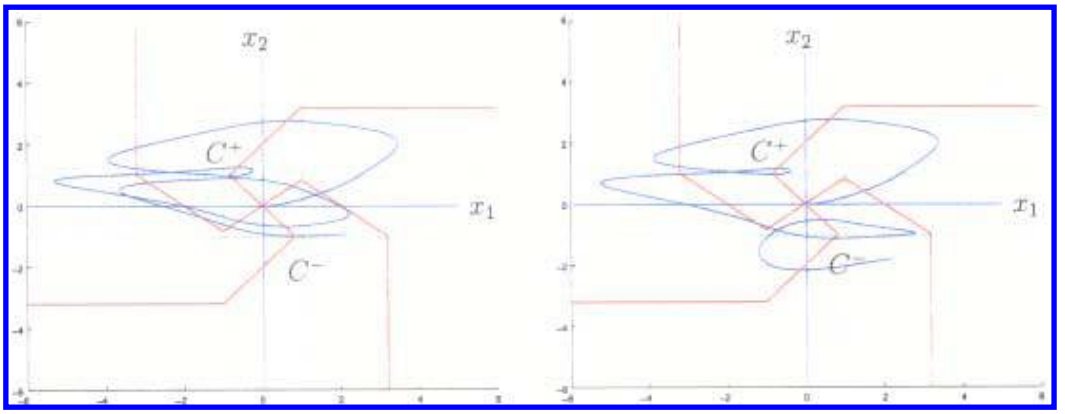

(c) $b_3^* = 4.365$ (d) $b^* = 4.2697$

Fig. 4. Critical trajectories of b_1^*, b_2^*, b_3^* and b^*, when $A = [1.2, 2, -1.2]$ and $T = 4$.

(2) Curve number ② decreases and curve number ③ increases and merges into $T_b/2$, giving rise to $4T$ periodic cycles. The $4T$ cycle will survive for quite a large range of parameters in (0.43, 0.66). Curves merging is very common and induces a period cycle.
(3) The $T_b/3$ mode maintains the largest parameters in (0, 3.826) and gives rise to a $3T$ periodic cycle in (1.2, 3.826).
(4) The dotted regions and window regions (stepped regions) interweave with each other. Stepped regions represent periodic cycles and dotted regions represent quasi-periodic orbits.

Section 5 will analyze the bifurcations before the onset of chaos.

In the ZN-case, when $b \geq 3.826$, the strength of the T-mode is comparable with or larger than the strength of the T_b-mode. In the following, a heuristic argument is used to derive relations among b, T and T_0 when T_b and T are comparable.

Let

$$\gamma(t) = \Lambda_0'(t + t_0)\,, \tag{28}$$

$\Lambda_0(t)$ be the limit cycle of (1) with $b = 0$. The first equation of (1) is modeled as

$$\frac{dx}{dt} = \gamma(t) + bu(t)\,. \tag{29}$$

Now, $\gamma(t)$ is a periodic function with period T_0 and $u(t)$ is a period function with period T. The two time scales of the functions γ and u can be normalized to a single time scale $\tau \in [0, 1]$ by setting $t = T_0\tau$ for γ and $t = T\tau$ for u. Hence,

$$x(t) = x(0) + T_0\Gamma(\tau) + bTU(\tau), \quad \tau \in [0, 1]\,, \tag{30}$$

where

$$\Gamma(\tau) = \int_0^{T_0\tau} \gamma(s)ds \quad \text{and} \quad U(\tau) = \int_0^{T\tau} u(s)ds$$

are normalized periodic functions with period one. From (30), $x(t)$ can vary maximally if T_0 and bT

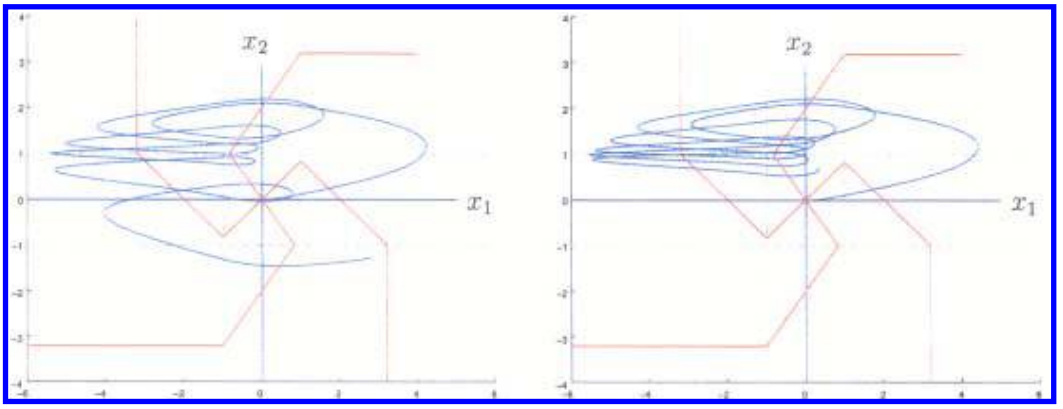

(a) $b = 8.44$ (b) $b = 8.9$

Fig. 5. Critical trajectories can circle around C^+ or C^- many times when $A = [1.2, 2, -1.2]$ and $T = 2$.

have the same order of magnitudes and an appropriate time shift t_0 occurs in (28). Therefore, for a fixed template $A = [r, p, s]$, let $T_0 = T_0(A)$ be the period of the sustained limit cycle $\Lambda_0(A)$ (without input), define

$$b^*(T) = \frac{c_0 T_0(A)}{T}\,, \tag{31}$$

where $c_0 \sim 1$ is a constant that depends on A and T.

From our experience, for a given A and T, $c_0 = 1$ in (31) is a good estimate for the position at which to start the search for interesting ranges of b. $c_0(A, T)$ may decrease as T increases. In the ZN-case and many other templates, (31) worked very well. See Figs. 4, 15 and 19.

The program (II) will be supported in Sec. 6, where asymptotic limit cycles Λ_∞ are studied as $b \to \infty$.

When the largest Lyapunov exponent of the Poincaré-map is close to zero and then becomes positive, (1) enters a chaotic region. In the ZN-case, eight chaotic regions C_k, $1 \le k \le 8$ can be identified, followed by successive window regions W_k, $1 \le k \le 8$. See Fig. 15. Bifurcations, typically backward period-doubling in window regions were discovered. See Fig. 16. Section 7 provides details. In the chaotic regions, three critical trajectories at b_1^*, b_2^*, and b_3^* can be identified which are important to implement program (III). See Figs. 4(a)–4(c). The parameter b_1^* is related to the onset of chaos while b_2^* and b_3^* are related to fully-developed chaos. They occur when T is near four in the ZN-case, but b_2^* and b_3^* may change considerably when T is relatively small, say $T \le 2$. In that case, b_2^* and b_3^* do not exist. Instead, the trajectories may circle around C^+ and C^- many times. See Fig. 5 and Sec. 7 for details.

When b is relatively large, in the ZN-case $b \ge 4.432$, the T-mode dominates, i.e. the sum of the strength of all other modes is less than a few percents of T-mode. The chaotic regions disappear and are followed by quasi-periodic regions and then, eventually, a periodic region. Now, Λ_b is either a symmetric or an asymmetric periodic cycle depending on T. Section 6 settles this issue by considering the asymptotic limit cycle Λ_∞ as $b \to \infty$.

4. Limit Cycles

This section addresses the existence and multiplicity of limit cycles of (1) when $b = 0$ and (3) holds.

The existence of limit cycles can be easily proven.

Theorem 4.1. *Assume (3) and $b = 0$, limit cycles exist. Moreover, apart from $O = (0, 0)$, all trajectories will tend to one of the limit cycles as $t \to \infty$.*

Proof. Under the assumptions (3), the origin $O = (0, 0)$ can be easily verified to be the only steady state of (1); moreover, O is an unstable spiral. Indeed, the associated eigenvalues at O are given by

$$\lambda_\pm = p - 1 \pm i\sqrt{-rs}\,.$$

By Theorem 2.2 and the Poincaré–Bendixson Theorem, a limit cycle exists. Apart from the origins, all trajectories will tend to one of the limit cycles as $t \to \infty$. The proof is complete. ■

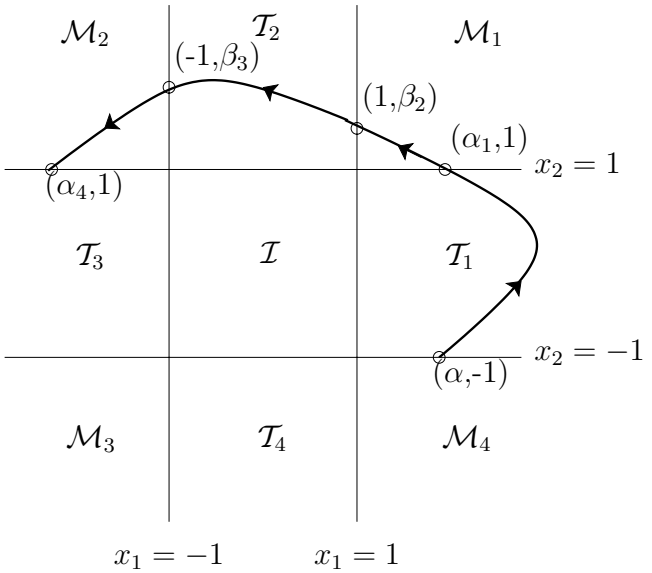

Fig. 6. A typical orbit of (1) with initial condition $(\alpha, -1)$, and $1 \le \alpha \le p - s$.

Since the nonlinear output function is piecewise linear in (2), the phase-plane can be divided into nine regions which are the mosaic (saturated) region $\mathcal{M}_j$, the transitional (partial saturated) region $\mathcal{T}_j$ and the interior (not saturated) region $\mathcal{I}$, $j = 1$, 2, 3, 4. See Fig. 6.

It is easy to see that the periodic orbit does not lie entirely in the interior region $\mathcal{I}$. Therefore, periodic orbits have to intersect the exterior region $\mathcal{E}$, here

$$\mathcal{E} = \mathbb{R}^2 - \mathcal{I} = \overline{\bigcup_{k=1}^{4} (\mathcal{T}_k \cup \mathcal{M}_k)}\,. \tag{32}$$

A periodic orbit Λ is called an exterior periodic cycle (exterior cycle) if $\Lambda \subseteq \mathcal{E}$, otherwise Λ is called a nonexterior periodic cycle, i.e. $\Lambda \bigcap \mathcal{I} \neq \emptyset$.

Now, the multiplicity of the exterior periodic cycles can be proven as follows.

Theorem 4.2. *Assume (3) and $b = 0$. No more than two limit cycles are present in the exterior region $\mathcal{E}$.*

Proof. Periodic solutions as in [Thiran, 1997] are constructed to show that no more than two periodic orbits exist in exterior region $\mathcal{E}$.

Now starting at the point $(\alpha, -1)$ at $t = 0$, where $1 \le \alpha \le p - s$, the trajectory Γ_α in $\mathcal{T}_1$ is followed; it intersects $x_2 = 1$ at the point $(\alpha_1, 1)$ on $t = t_1$, $1 < \alpha_1$, enters $\mathcal{M}_1$; then intersects $x_1 = 1$ at $(1, \beta_2)$ on $t = t_2$, enters $\mathcal{T}_2$; then intersects $x_1 = -1$ at the point $(-1, \beta_3)$ on $t = t_3$, and finally enters $\mathcal{M}_2$ and intersects $x_2 = 1$ at the point $(\alpha_4, 1)$ on $t = t_4$, i.e.

$$\begin{aligned}
&(x_1(0), x_2(0)) = (\alpha, -1)\,,\\
&(x_1(t_1), x_2(t_1)) = (\alpha_1, 1)\,,\\
&(x_1(t_2), x_2(t_2)) = (1, \beta_2)\,,\\
&(x_1(t_3), x_2(t_3)) = (-1, \beta_3)\,,\\
&(x_1(t_4), x_2(t_4)) = (\alpha_4, 1)\,.
\end{aligned} \tag{33}$$

See Fig. 6. Since $b = 0$, (1) is an autonomous equation. The periodic orbit cannot intersect itself. Therefore, by Theorem 2.1(i), Γ_α is a periodic (closed) orbit if and only if

$$\alpha_4 = -\alpha\,. \tag{34}$$

α_1, β_2, β_3, α_4 and t_1, t_2, t_3, t_4 must be computed in terms of α. The following expressions can be straight-forwardly obtained. The details are omitted here. Denote by

$$\begin{aligned}
&\xi = r + 1 - p, \quad \eta = r + p - 1\,,\\
&\gamma = 1 - s - p, \quad \delta = p - s - 1\,,\\
&\text{and} \quad q = 1/(p-1)\,.
\end{aligned} \tag{35}$$

Then,

$$\alpha_1 = p + \frac{s(1-r)}{p} + \left(\alpha - p + \frac{s(r+1)}{p}\right)\left(\frac{\xi}{\eta}\right)^q\,, \tag{36}$$

$$\beta_2 = p + r - \frac{\eta\gamma}{\alpha_1 - p - s}\,, \tag{37}$$

$$\beta_3 = p - \frac{r(s+1)}{p} + \left(\beta_2 - p - \frac{r(1-s)}{p}\right)\left(\frac{\gamma}{\delta}\right)^q\,, \tag{38}$$

$$\alpha_4 = \frac{\delta\xi}{\beta_3 + r - p} + s - p\,. \tag{39}$$

α_4 is written as a function of α to show that (34) has at most two solutions for $\alpha \in [1, p - s]$. Indeed, in the following, k_i, $i = 1, \ldots, 17$, are constants that depend on p, r, s, but are independent of α,

$$\begin{aligned}
\alpha_1 &= k_1\alpha + k_2\,,\\
\beta_2 &= \frac{k_4}{k_1\alpha + k_3} + k_5\,,\\
\beta_3 &= k_6\beta_2 + k_7\,,\\
\alpha_4 &= \frac{k_9}{\beta_3 + k_8} + k_{10}\,,
\end{aligned}$$

and

$$\alpha_4 = \frac{k_9\alpha + k_{13}}{k_{11}\alpha + k_{12}} + k_{14}\,. \tag{40}$$

Substituting (40) into (34) yields, a quadratic equation for α, i.e.

$$k_{15}\alpha^2 + k_{16}\alpha + k_{17} = 0\,. \tag{41}$$

Therefore, (34) has at most two solutions in $[1,\, p-s]$. The proof is complete. ■

The uniqueness of limit cycle in the exterior region $\mathcal{E}$ can be proven by making further assumptions:

Theorem 4.3. *Assume (3) and $b = 0$. If $1 < p \le 2$ then (1) has at most one limit cycle in the exterior region $\mathcal{E}$.*

Proof. Note that

$$\frac{\partial}{\partial x_1}(-x_1 + py_1 + sy_2) + \frac{\partial}{\partial x_2}(-x_2 + ry_1 + py_2)$$
$$= \begin{cases} p-2 & \text{if } (x_1,\, x_2) \in \mathcal{T}_i\,, \\ -2 & \text{if } (x_1,\, x_2) \in \mathcal{M}_i\,, \end{cases}$$

$1 \le i \le 4$. The sign is nonpositive if $p \le 2$. The Dulac criteria rule out the second closed orbit in $\mathcal{E}$. The proof is complete. ■

The existence and nonexistence of periodic cycles in the exterior region $\mathcal{E}$ can also be proven by making additional assumptions.

Theorem 4.4. *Assume (3) and $b = 0$. Let ξ, η, γ, δ and q be given by (35).*

(i) *There is a periodic cycle in the exterior region $\mathcal{E}$ if the following conditions are satisfied.*

$$(E_1)\quad p - 1 + \frac{s(1-r)}{p} + \left(1 - p + \frac{s(r+1)}{p}\right)\left(\frac{\xi}{\eta}\right)^q \ge 0\,, \tag{42}$$

$$p - 1 - \frac{r(1+s)}{p} + \left(1 - p - \frac{r(1-s)}{p}\right)\left(\frac{\gamma}{\delta}\right)^q \ge 0\,. \tag{43}$$

In particular, if A is antisymmetric, i.e. $-s = r$, (E_1) and (E_2) are equivalent to

$$(E)\quad p(p-1) + r(r-1) - [p(p-1) + r(r+1)]\left(\frac{\xi}{\eta}\right)^q \ge 0\,. \tag{44}$$

(ii) *There is no periodic orbit in the exterior region $\mathcal{E}$ if one of the following conditions holds.*

$$(N_1)\quad p - 1 + \frac{s(1-r)}{p} + \frac{s\xi}{p}\left(\frac{\xi}{\eta}\right)^q < 0\,, \tag{45}$$

or

$$(N_2)\quad p - 1 - \frac{r(1+s)}{p} - \frac{r\gamma}{p}\left(\frac{\gamma}{\delta}\right)^q < 0\,. \tag{46}$$

In that case, all periodic cycles necessarily intersect the interior region $\mathcal{I}$.

Proof. The existence results are first proved.

It is easy to verify that if Λ is an exterior periodic cycle then $\Lambda \bigcap \{(x_1, -1) | x_1 \in [1,\, p-s]\} \ne \emptyset$.

From (36) and (42),

$$\alpha_1(\alpha) \ge 1 \quad \text{for all} \quad \alpha \in [1,\, p-s]\,. \tag{47}$$

Similarly, from (38) and (43),

$$\beta_3(\beta_2) \ge 1 \quad \text{for all} \quad \beta_2 \in [1,\, p+r]\,. \tag{48}$$

Therefore, $x_1(\alpha,\, 1)$ maps $[1,\, p-s]$ into $[-p+s,\, -1]$. It implies $-x_1(\alpha,\, 1)$ maps $[1,\, p-s]$ into itself and then has a fixed point in $[1,\, p-s]$. Hence, (34) has at least one solution in $[1,\, p-s]$. This proves that exterior periodic cycle exists.

Clearly, (E_1) and (E_2) is equivalent to (E) when $s = -r$.

Finally, from (36) and (45),

$$\alpha_1(\alpha) < 1 \quad \text{for all} \quad \alpha \in [1,\, p-s]\,, \tag{49}$$

and from (38) and (46),

$$\beta_3(\beta_2) < 1 \quad \text{for all} \quad \beta_2 \in [1,\, p+r]\,. \tag{50}$$

Hence, there no exterior periodic cycle exists. The proof is complete. ■

Notably, (45) and (46) can be replaced by stronger conditions that can be verified easily as follows.

$$0 < p - 1 < r < 1 \quad \text{and} \quad -s \ge \frac{p(p-1)}{1-r}\,, \tag{51}$$

and

$$0 < p - 1 < -s < 1 \quad \text{and} \quad r \ge \frac{p(p-1)}{1+s}\,. \tag{52}$$

Figure 7 shows some typical exterior periodic cycles and nonexterior periodic cycles.

Although, the expressions (36)–(39) are explicit, analytically showing that (41) has a unique solution in exterior region $\mathcal{E}$ remains quite difficult.

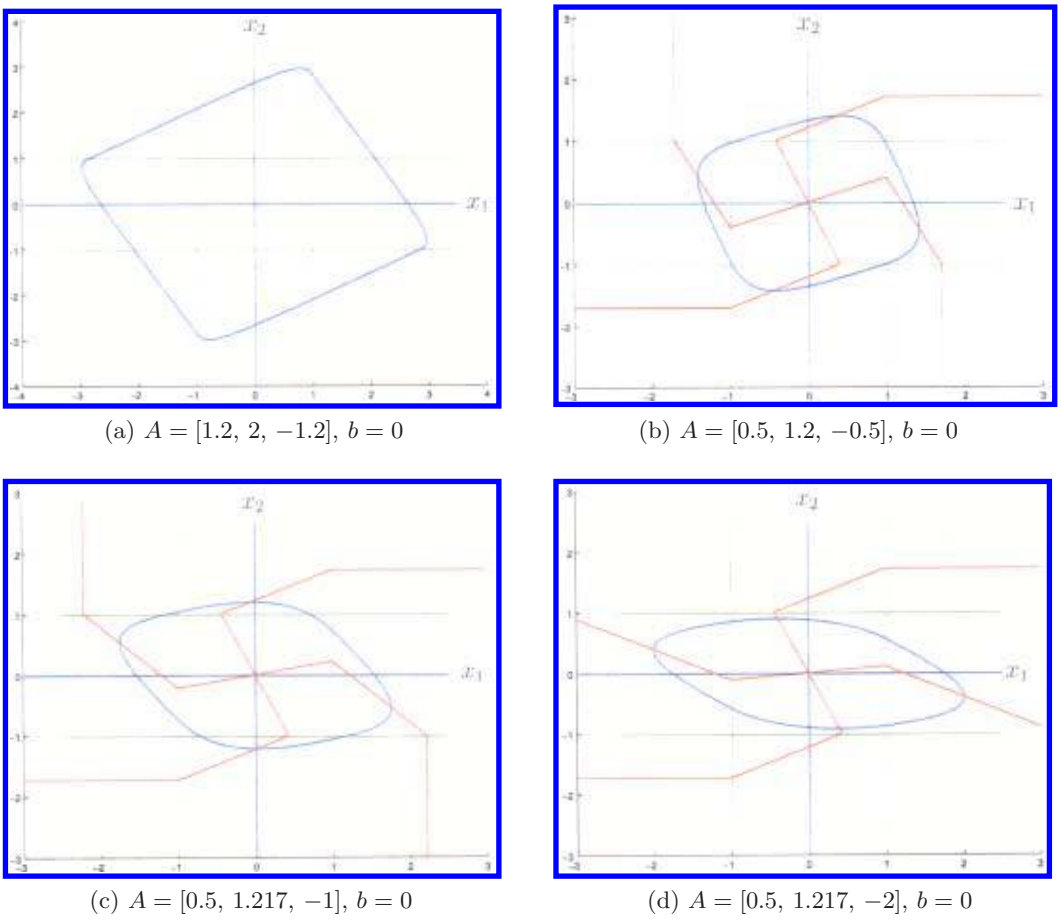

(a) $A = [1.2, 2, -1.2]$, $b = 0$ (b) $A = [0.5, 1.2, -0.5]$, $b = 0$

(c) $A = [0.5, 1.217, -1]$, $b = 0$ (d) $A = [0.5, 1.217, -2]$, $b = 0$

Fig. 7. Typical limit cycles of (1) with $b = 0$, (a) exterior cycle, (b)–(d) nonexterior cycles.

However, numerical results indicate that a unique limit cycle exists in the entire $\mathbb{R}^2$ over a quite large parameter range.

Numerical computation also reveals, the period function $T_0(r, p, s)$ of the limit cycles for template $A = [r, p, s]$ that satisfies the condition (3) is decreasing with respect to r and $-s$, and increasing with respect to p. See Figs. 8 and 9. An analytic study of this monotonicity has some progress.

5. Bifurcations Precede Chaos

This section considers the bifurcations before chaos when the amplitude b of the input is relatively small. Section 3 explains the methods used.

Given a template A which satisfies (3), assume that (1) has a unique limit cycle $\Lambda_0(A)$ with period $T_0 = T_0(A)$. For each $T \in (0, T_0)$ and $b > 0$, let $T_b = T(b, T, A)$ be the period of the largest amplitude $a_1(b, T, A)$ of the FFT except for T-mode applied to $x_1(t, 0, 0; b, T, A)$ and let $a_T(b, T, A)$ be the amplitude of T-mode. Let $b_0^* > 0$ such that

$$|a_1(b, T, A)| > |a_T(b, T, A)| \tag{53}$$

holds in $(0, b_0^*)$, b_0^* can be assumed to be the least upper bound of $\tilde{b}$ such that (53) holds in $(0, \tilde{b})$.

Consider the first N highest modes and plot the curves

$$R_k(b) \equiv \frac{\tau_k(b)}{T_b} \tag{54}$$

for $b \in (0, b_0^*)$ and $k = 1, \ldots, N$, where $\tau_k(b)$ is the period of the kth-largest amplitude of the FFT and $T_b = \tau_1(b)$. See Fig. 3. The $R_k(b)$ curve is well defined locally in the window regions and can merge with its neighbor curves. After they merge, they are considered to be one curve. See curves ② and ③ in Fig. 3.

When a periodic window appears on the open interval $B \subset (0, b_0^*)$, the curve $R_k(b)$ will be a horizontal line, or approximately one, on B.

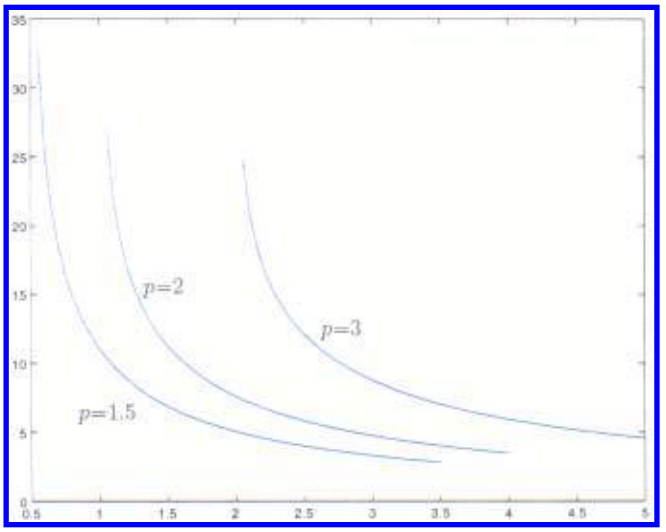

Fig. 8. The period function $T_0(r, p, -r)$ with $b = 0$.

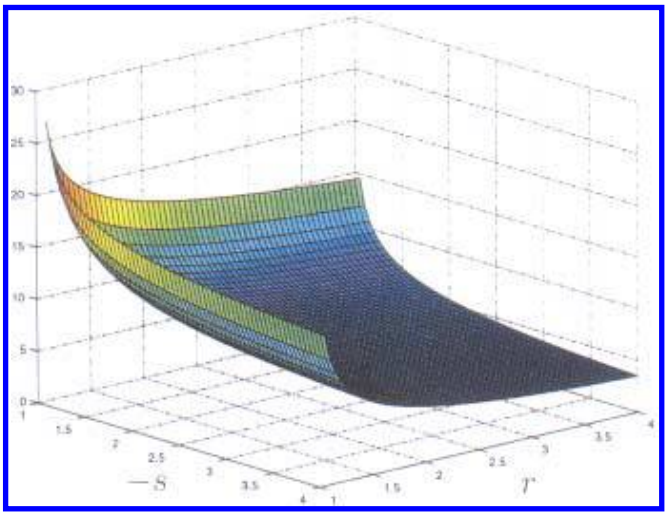

Fig. 9. The period function $T_0(r, 2, s)$ with $b = 0$.

Furthermore, on B

$$T_b = \frac{m}{n}T \tag{55}$$

for some positive integers m and n and $(m, n) = 1$, i.e. m and n are relative prime. Therefore,

$$B_{m,n} = \left\{ b \in (0, b_0^*) | T_b = \frac{m}{n}T \right\} \tag{56}$$

is defined. Denote by

$$[T_0/T] = m^* , \tag{57}$$

where $[x]$ is the largest integer which is equal to or smaller than x.

The solutions of (1) can be written explicitly on each of the nine regions $\mathcal{M}_j$, $\mathcal{T}_j$ and $\mathcal{I}$. Therefore, the exact solutions of periodic orbits in $B_{m,n}$ can be rigorously checked using a computer provided n is not too large. The periodic cycles in $B_{m,n}$ are of period mT and circle around the origin O n-times (n-copies). This explanation partially proves the following results.

Conjecture 5.1. *Assume (53) holds. Then*

(i) $B_{m^*,1} \neq \emptyset$, *i.e. a stable* m^*T *periodic cycle of (1) exists.*

(ii) *If (1) has another stable limit cycle with* m_*T *period in* $B_{m_*,n_*} \subset (0, b_0^*)$ *and* $m_*/n_* < m^*$, *then* $\cup_{m_*/n_* \leq m/n \leq m^*} B_{m,n}$ *is open and dense in* $(\hat{b}_1, \hat{b}_2)$, *where* $\hat{b}_1 = \inf B_{m^*,1}$ *and* $\hat{b}_2 = \sup B_{m_*,n_*}$, *i.e.* T_b *is a function of* b *is a devil's staircase in* b. *See Fig. 10.*

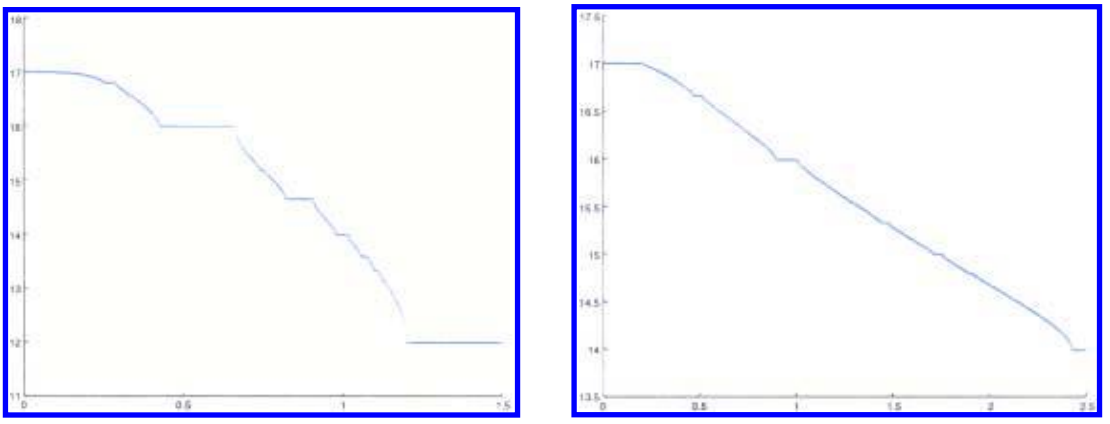

(a) $T = 4$ (b) $T = 2$

Fig. 10. Devil's staircase like period function T_b, $A = [1.2, 2, -1.2]$, (a) $T = 4$ and (b) $T = 2$.

Figure 11 plots the typical periodic orbits in $B_{m,n}$ in the ZN-case and Fig. 12 plots the typical quasi-periodic orbits in the ZN-case.

6. Asymptotic Limit Cycles for Large Inputs

This section addresses asymptotic periodic cycles for various T when b is large. Whether the ω-limit sets ω_b and $-\omega_b$ can be separated from each other by the x_1-axis such that one lies in the upper half of phase-plane and the other lies in the lower half of phase-plane is the main concern. The answer is affirmative when T is relatively small. See Theorem 6.1. In any case, the system can always support a limiting cycle even for large T.

For a given template $A = [r, p, s]$,

$$w_1 = \frac{x_1}{b} \tag{58}$$

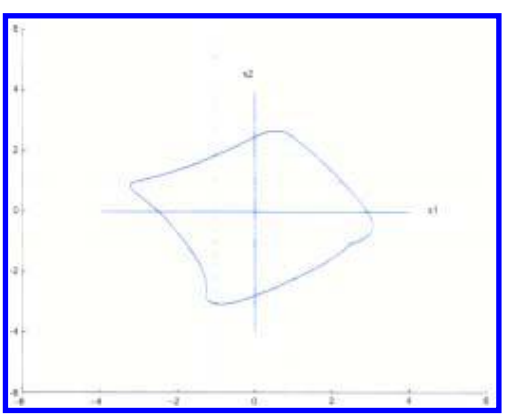

(a) $b = 0.5$, $T_b = 4T$

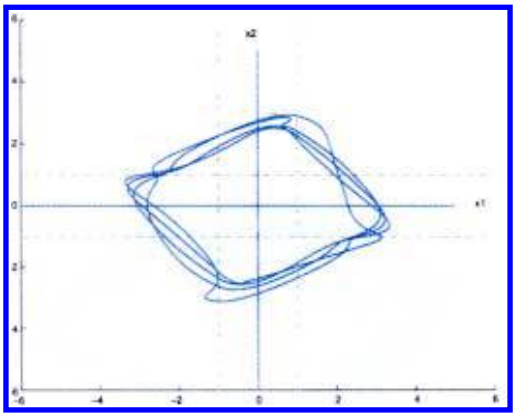

(b) $b = 0.78$, $T_b = \frac{15}{4}T$

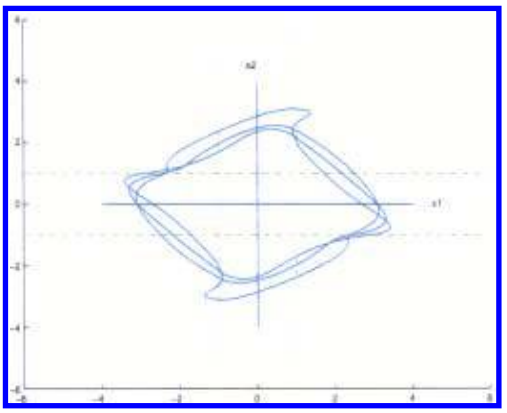

(c) $b = 0.9$, $T_b = \frac{11}{3}T$

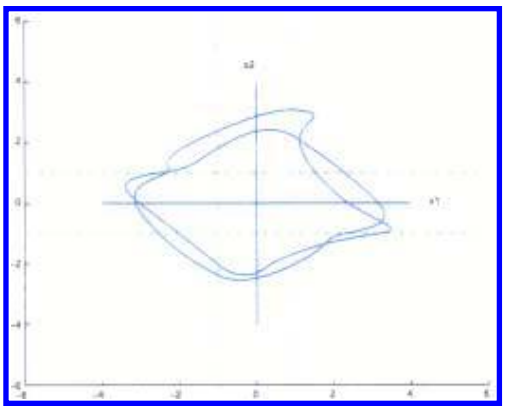

(d) $b = 1$, $T_b = \frac{7}{2}T$

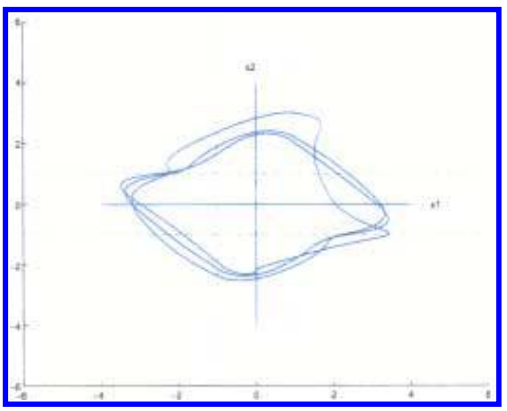

(e) $b = 1.1$, $T_b = \frac{10}{3}T$

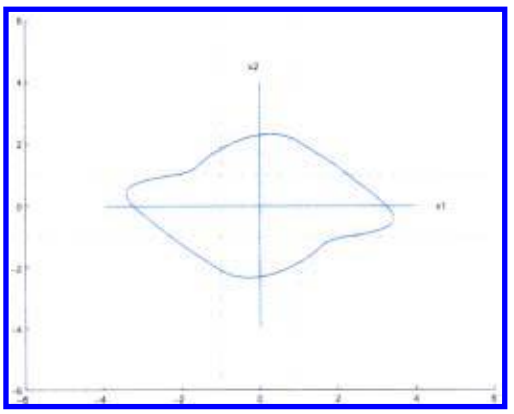

(f) $b = 1.2$, $T_b = 3T$

Fig. 11. Some typical orbits in $B_{m,n}$ prior to chaotic regions, $A = [1.2, 2, -1.2]$ and $T = 4$.

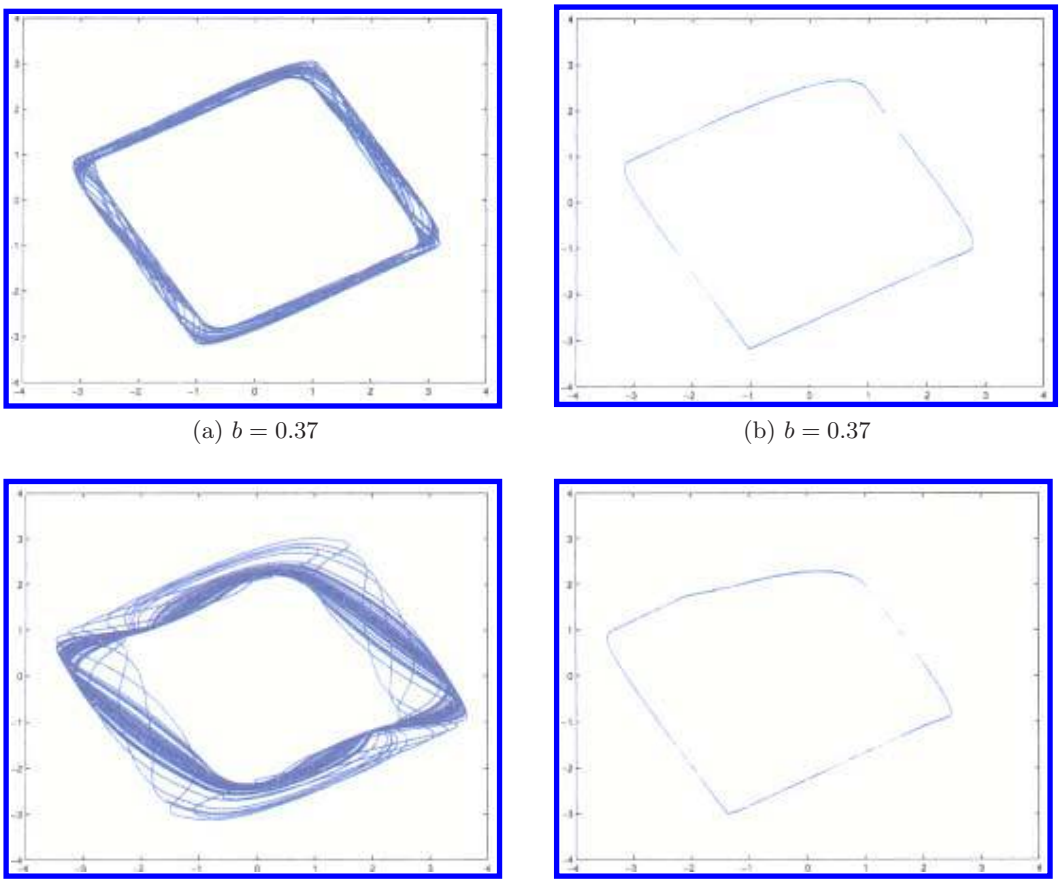

(a) $b = 0.37$ (b) $b = 0.37$

(c) $b = 1.14$ (d) $b = 1.14$

Fig. 12. Some typical quasi-periodic orbit (a) and (c) and their ω-limit set $\hat{\omega}$ of the Poincaré map (b) and (d), $A = [1.2, 2, -1.2]$ and $T = 4$.

is written as $b \to \infty$, and the limiting equation for w_1 is

$$\frac{dw_1}{dt} = -w_1 + u\,. \tag{59}$$

The solutions of (59) are

$$w_1(t) = ce^{-t} + \frac{1}{1+\Omega^2}(\sin\Omega t - \Omega\cos\Omega t)\,, \tag{60}$$

where

$$\Omega = \Omega(T) = \frac{2\pi}{T}$$

and c is a constant. Consequently,

$$x_1(t, \xi_1, \xi_2; b) \sim \frac{b}{1+\Omega^2}(\sin\Omega t - \Omega\cos\Omega t) \tag{61}$$

for large b and t. Notably,

$$-p - r < x_2(t, \xi_1, \xi_2; b) < p + r \tag{62}$$

always holds for large t. Now, (1) is assumed to have a asymptotic limit cycle Λ_∞ with period T as $b \to \infty$. From (61), Λ_∞ will always almost be in the region $|x_1| \geq 1$. In the limit, denoted by $w_2(t)$ for $x_2(t; b)$, w_2 satisfies

$$\frac{dw_2}{dt} = -w_2 + p + r \quad \text{if} \quad w_2 \geq 1\,, \tag{63}$$

$$\frac{dw_2}{dt} = (p-1)w_2 + r \quad \text{if} \quad |w_2| \leq 1\,, \tag{64}$$

$$\frac{dw_2}{dt} = -w_2 + r - p \quad \text{if} \quad w_2 \leq -1\,. \tag{65}$$

for a total time of $T/2$ in the region $w_1 \geq 0$. Similar equations hold in region $w_1 \leq 0$ for another $T/2$ time. The separation theorem is stated as follows.

Theorem 6.1. *The system (1) can support a limiting limit cycle Λ_∞ with period T provided*

(i) *in region $w_2 \leq -1$ if*

$$T < T_1^* \equiv 2\log\frac{2r}{r+1-p}\,, \tag{66}$$

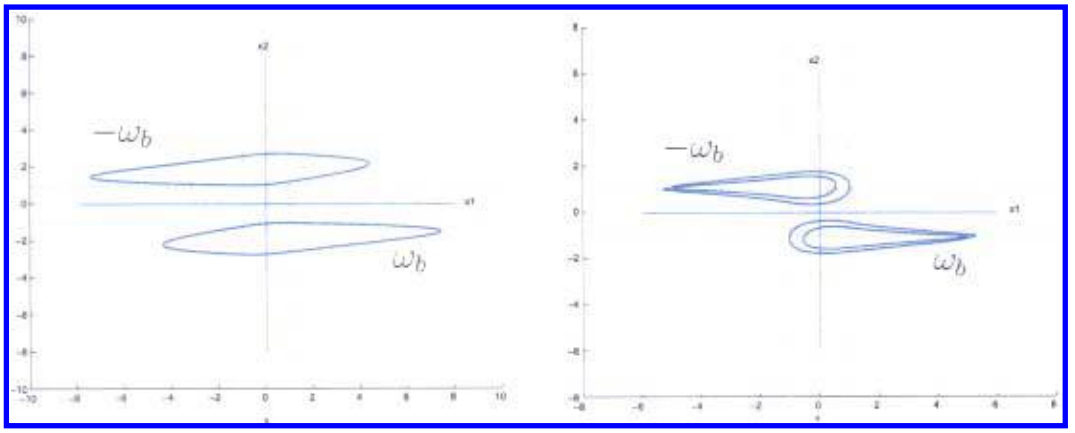

(a) $b = 10$ (b) $b = 4.8$

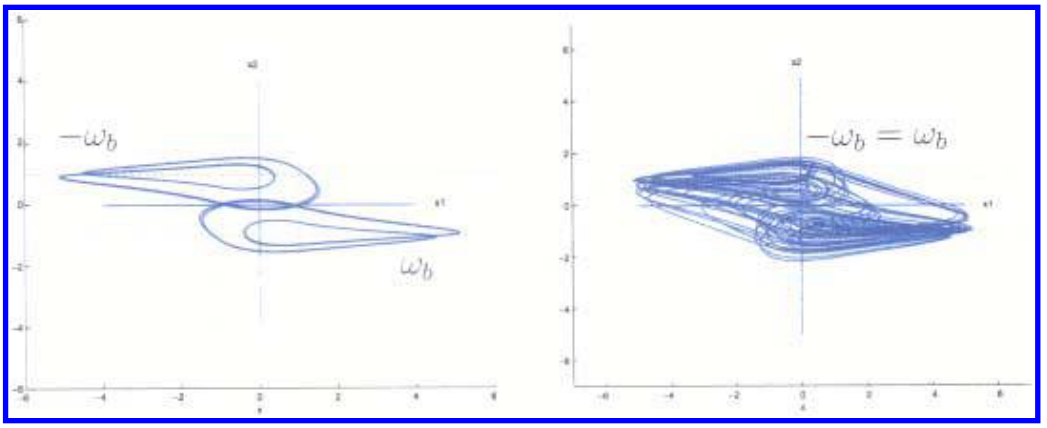

(c) $b = 4.428$ (d) $b = 4.336$

Fig. 13. Crises induced by ω_b and $-\omega_b$ when $A = [1.2,\ 2,\ -1.2]$ and $T = 4$.

(ii) *in region* $w_2 \le 0$ *if*

$$T < T_0^* \equiv 2\left(\log\frac{2r}{r+1-p} + \frac{1}{p-1}\log\frac{r}{r+1-p}\right). \tag{67}$$

Similarly, $-\Lambda_\infty$ *lies in* $w_2 \ge 1$ *and* $w_2 \ge 0$, *respectively.*

Proof

(i) Assume that Λ_∞ remains in the region $w_2 \le -1$ for $T/2$ time. Then general solutions of (65) are

$$w_2(t) = ce^{-t} + r - p\,. \tag{68}$$

For $1 \le \beta \le \alpha < p + r$, assume

$$w_2(t_0) = -\alpha\,, \quad \text{and} \quad w_2\left(t_0 + \frac{T}{2}\right) = -\beta\,. \tag{69}$$

Then (68) and (69) imply

$$T = 2\log\frac{\alpha + r - p}{\beta + r - p}\,. \tag{70}$$

Since $1 \le \beta \le \alpha < p + r$, (66) follows.

(ii) Assume that Λ_∞ remains in the region $w_2 \le 0$ for $T/2$ time. Let

$$\begin{aligned} 0 \le \beta \le 1 \le \alpha < p + r\,,\\ w_2(t_0) = -\alpha\,,\\ w_2(t_0 + T') = -1\,,\\ w_2\left(t_0 + \frac{T}{2}\right) = -\beta\,, \end{aligned} \tag{71}$$

where $0 < T' < T/2$. Then from (64) and (65),

$$w_2(t) = c_1 e^{-t} + r - p \quad \text{for} \quad t \in [t_0,\, t_0 + T']\,, \tag{72}$$

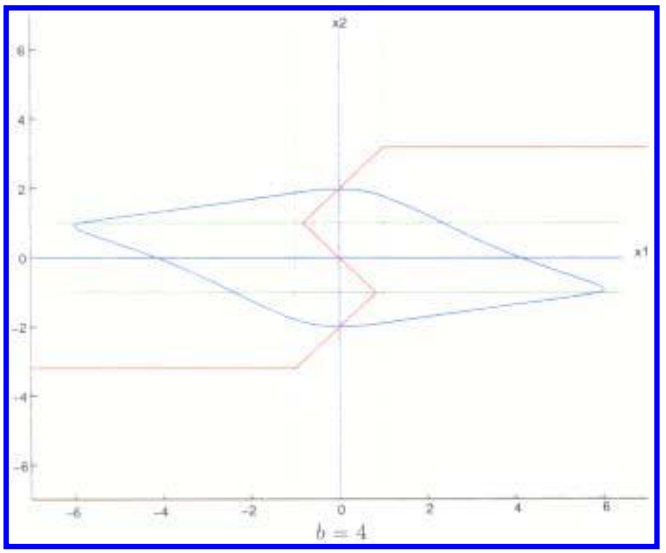

Fig. 14. ω_b=$-\omega_b$ when $A = [1.2, 2, -1.2]$ and $T = 10$.

and

$$w_2(t) = c_2 e^{(p-1)t} - \frac{r}{p-1} \quad \text{for} \quad t \in \left[t_0 + T', t_0 + \frac{T}{2}\right]. \tag{73}$$

From (72),

$$T' = \log \frac{\alpha + r - p}{1 + r - p}. \tag{74}$$

Similarly, from (71) and (73),

$$\frac{T}{2} - T' = \frac{1}{p-1} \log \frac{r - \beta(p-1)}{r + 1 - p}. \tag{75}$$

From (74) and (75),

$$T = 2\left\{\log \frac{\alpha + r - p}{r + 1 - p} + \frac{1}{p-1} \log \frac{r - \beta(p-1)}{r + 1 - p}\right\}$$

which implies (67).

The proof is complete. ■

Remark 6.2

(i) The perturbation method can be used to prove that there exists a limit cycle Λ_b with period T for large b. Λ_b lies in the region according to Theorem 6.1. The details are omitted here. See Fig. 13.

(ii) For large T, Λ_∞ can be proven to exist with period T. Furthermore, Λ_∞ spends most of $T/2$ time near $p+r$. Therefore, for large T and large b, Λ_b is a symmetric T-periodic cycle like a rhombus, with two vertices close to $(1, p + r)$ and $(-1, -p - r)$, respectively. See Fig. 14.

Remark 6.3. When T satisfies either (66) or (67), Λ_∞ and $-\Lambda_\infty$ are separated. Then Λ_b and $-\Lambda_b$ are also separated when b is large. For example, in the ZN-case i.e. $A = [1.2, 2, -1.2]$,

$$T_1^* = 4.9698 \tag{76}$$

and

$$T_0^* = 8.5533. \tag{77}$$

Note that $T = 4 < T_1^*$ has been used in [Zou & Nossek, 1991], when b decreases to some critical number b_∞^*, ω_b and $-\omega_b$ cross each other and cause crises; chaos may occur when b decreases a little further. See Figs. 13(a)–13(d). If T is too large, chaos may not occur, for example, in the ZN-case $A = [1.2, 2, -1.2]$ and $T = 10$, in that case, ω_b is like rhombus. See Fig. 14.

7. Chaos

This section considers the chaotic phenomena that occurs when the strengths of Γ_b and the input bu are comparable. A specific model of the ZN-case is studied first to elucidate the methods of the study and the chaotic behavior. Section 7.1 addresses bifurcation to chaos by fixing the template A and the input period T and varying the amplitude b. Section 7.2 considers the effect of an input period T by fixing the template A. The asymptotic limit cycles Λ_∞ studied in Sec. 6 will guide the approach taken to solving the problem. Section 7.3 addresses the fundamental role of the template A.

7.1. *Effects of input amplitude*

As stated in Sec. 3, ω_b is a chaotic attractor if the following three conditions are satisfied.

(i) $\Gamma(b, T, A)$ has a positive Lyapunov exponent,
(ii) $\hat{\omega}(b, T, A)$ is fractal,
(iii) $\Gamma(b.T, A)$ has a broad-band in FFT.

The numerical methods for computing Lyapunov exponents, Poincaré maps and FFTs are standard and have been applied by many researchers. Section 8 will detail these methods. In all cases studied, the largest Lyapunov exponents must exceed 0.02 to be considered to be positive. When $\hat{\omega}_b$ appears as a partial lady's shoe or as a horseshoe, it is considered to be fractal. Quantitative results concerning fractal dimensions can also

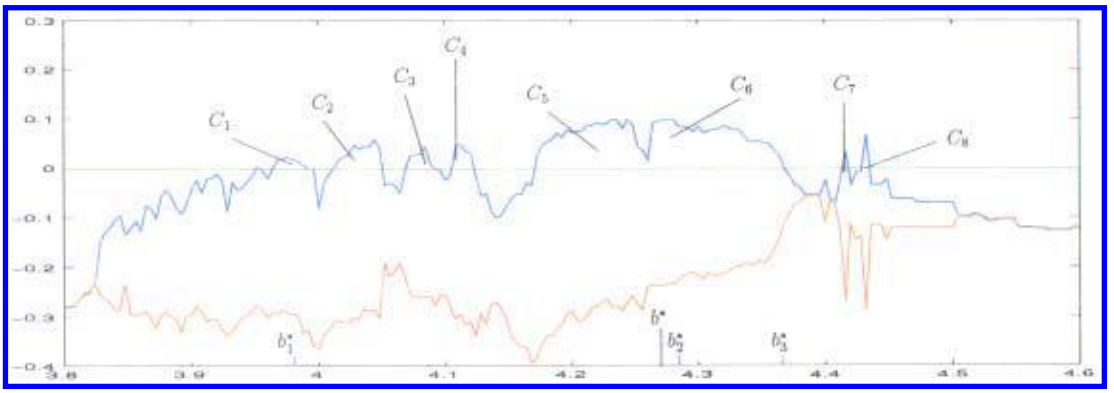

Fig. 15. Lyapunov exponents diagram for the ZN-case with b in (30) and (37), $b_1^* = 3.98$, $b_2^* = 4.284$, $b_3^* = 4.365$ and $b^* = 4.2697$.

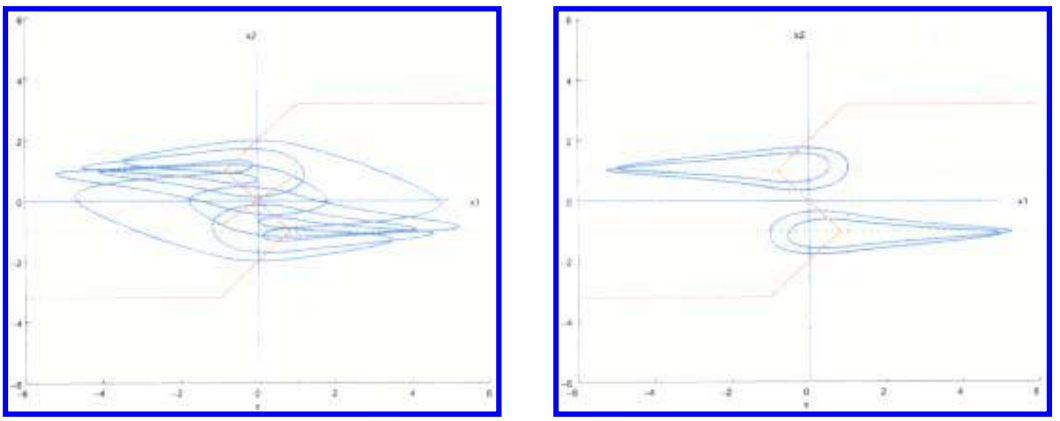

(a) Type I (b) Type II

Fig. 16. (a) Type I: the orbit Γ_b circles around all three points C^+, O and C^-. (b) Type II: the orbit Γ_b does not circle around all of three points C^+, O and C^-.

be computed in these cases. Finally, the broad-band of FFT is considered in the classical sense.

The ZN-case, with $A = [1.2, 2, -1.2]$ and $T = 4$, is first considered as a model to help discuss the bifurcations of chaotic phenomena. The Lyapunov exponents were computed for a long $b > 0$.

Table 1.

Characteristics	(1)	(2)	(3)	(4)	(5)
W_0	(3.956, 3.96)	7	a	T	I
W_1	(3.992, 4.008)	11	s	T_b	I
W_2	(4.052, 4.068)	6	a	T	I
W_3	(4.092, 4.104)	10	a	T	I
W_4	(4.124, 4.168)	4	a	T_b	I
W_5	(4.252, 4.260)	9	s	T	I
W_6	(4.368, 4.412)	8	a	T	I
W_7	(4.42, 4.431)	4	a	T	II
W_8	(4.433, ∞)	2	a	T	I

The largest Lyapunov exponent that is close to or above zero is recorded in $b \in (3.8, 4.6)$. See Fig. 15. It can be used to identify eight regions C_k, $1 \leq k \leq 8$, which are chaotic since they have positive Lyapunov exponents. Notably, C_4 is the region that has been studied by Zou and Nossek [1991]. Each chaotic region C_k is followed by a window region W_k and $1 \leq k \leq 8$. The window W_0 precedes C_1.

In each W_k and $0 \leq k \leq 8$, the basic periodic cycle — the periodic solutions with the smallest period — can be identified. These windows are first compared in terms of the following characteristics of the basic periodic cycle in each W_k.

(1) Range of parameters in window,
(2) Period in T units,
(3) Symmetry: "s" for symmetric and "a" for asymmetric cycles,

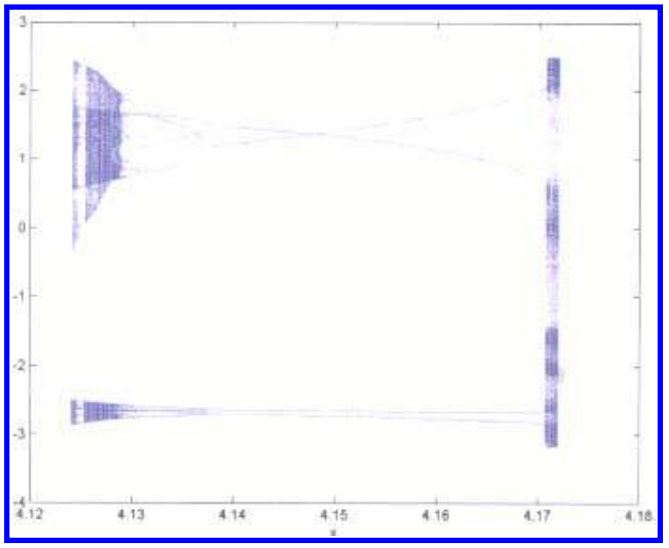

Fig. 17. Bifurcations diagram for ZN-case with b in window $W_4 = (4.124, 4.172)$.

(4) Dominating mode in FFT: T_b for superiority of T_b and T for input,
(5) Type of attractor: "I" for type I, "II" for type II. See Figs. 16(a) and 16(b).

Considering W_k carefully, for example, in W_4, reveals that at the middle point of (4.124, 4.168) the $4T$ basic periodic cycle is asymmetric. To its left, a sequence of periodic-doubling occurs; to its right is a quasi-periodic region. See Fig. 17. Similarly, W_5 includes a symmetric $9T$ basic periodic cycle, with periodic-doubling to its left and a quasi-periodic region to its right.

To analyze ω_b in C_k, it is considered to be a chaotic bifurcation from different types of windows W_{k-1} and W_k. $\hat{\omega}_b$ of the Poincaré map in C_k will track the change of the basic periodic orbits $\hat{\omega}_b$ in W_{k-1} and W_k. See Figs. 18(a)–18(n) for the

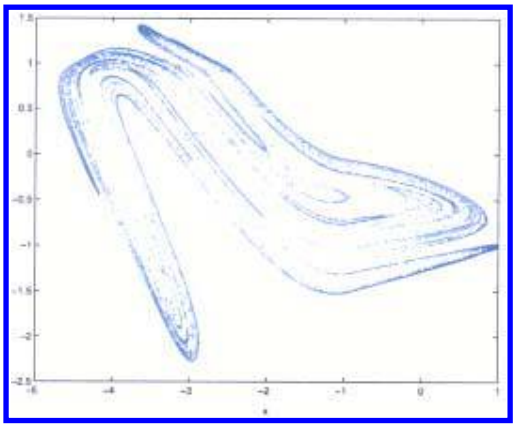

(a) $b = 3.976 \in C_1$

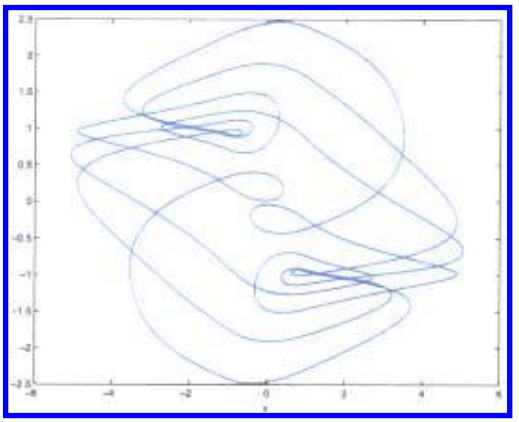

(b) $b = 3.996 \in W_1$

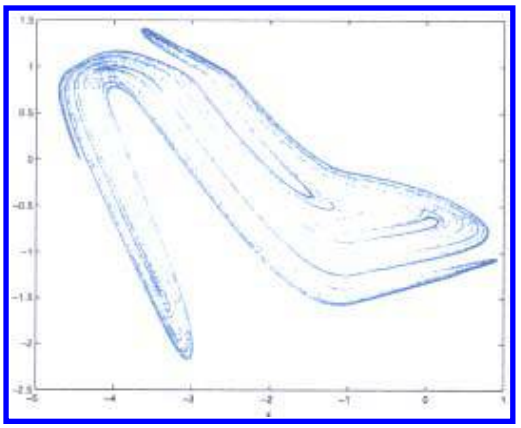

(c) $b = 4.04 \in C_2$

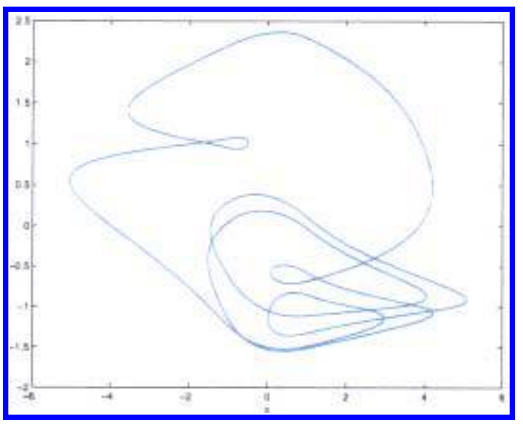

(d) $b = 4.056 \in W_2$

Fig. 18. Typical Poincaré section in chaotic regions and basic periodic cycles in windows, $A = [1.2, 2, -1.2]$ and $T = 4$.

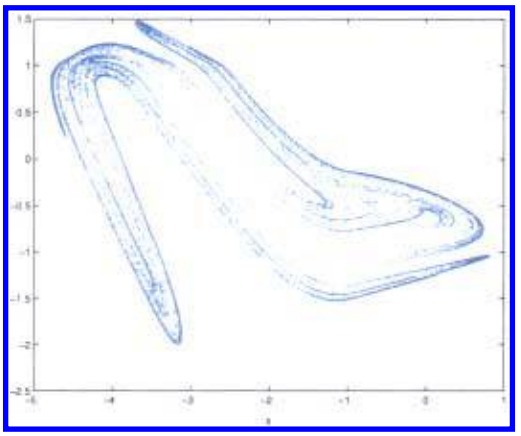

(e) $b = 4.084 \in C_3$

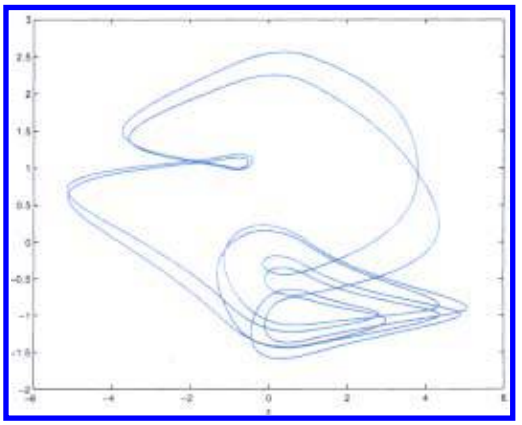

(f) $b = 4.104 \in W_3$

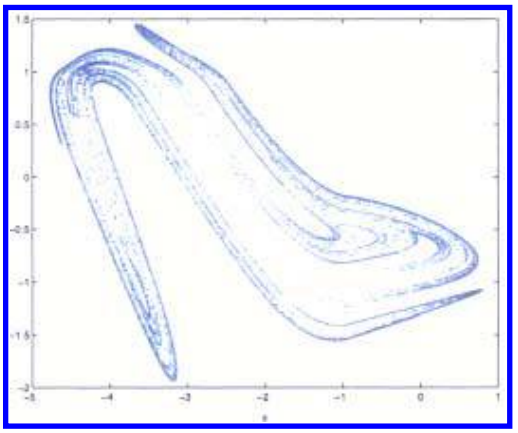

(g) $b = 4.112 \in C_4$

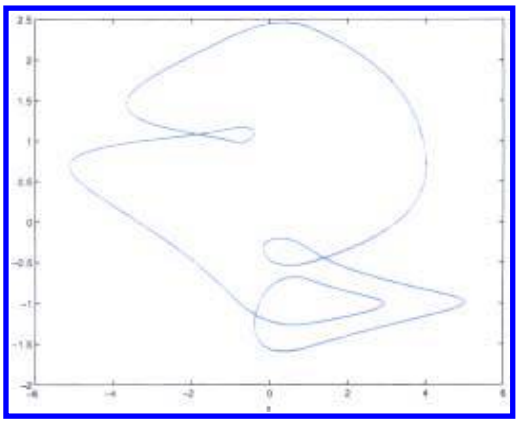

(h) $b = 4.144 \in W_4$

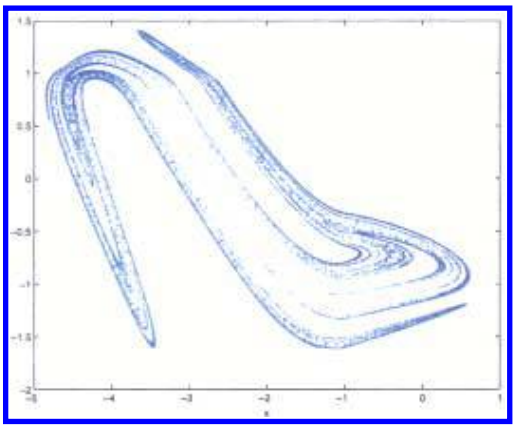

(i) $b = 4.204 \in C_5$

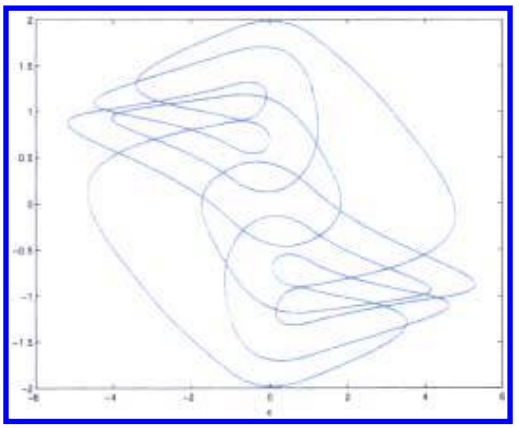

(j) $b = 4.256 \in W_5$

Fig. 18. (*Continued*)

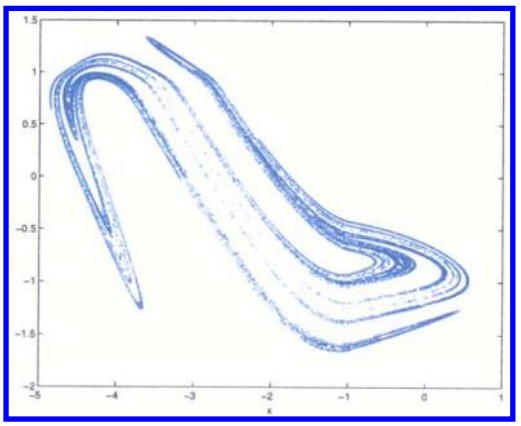

(k) $b = 4.264 \in C_6$

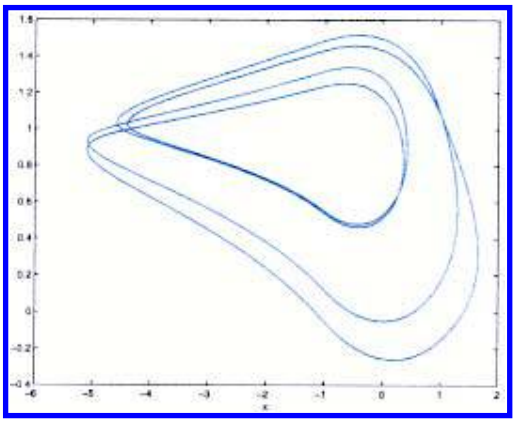

(l) $b = 4.412 \in W_6$

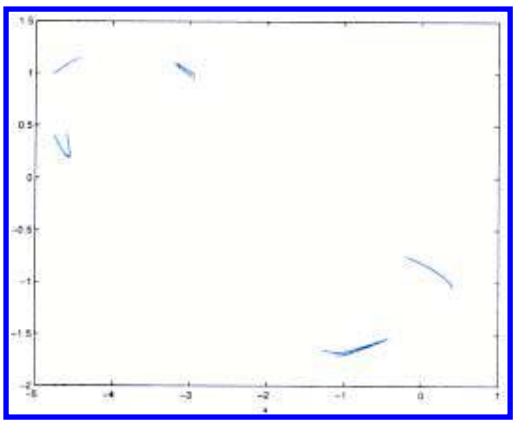

(m) $b = 4.416 \in C_7$

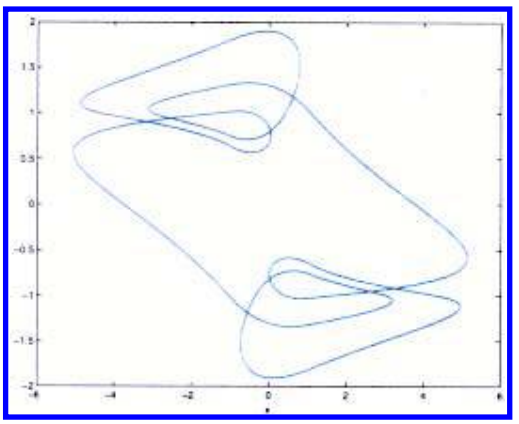

(n) $b = 4.42 \in W_7$

Fig. 18. (*Continued*)

transitions. Notably, the basic periodic cycles in windows W_k like those in Fig. 18, which circle around C^+, O and C^-, differ greatly from the periodic cycles in $B_{m,n}$ as shown in Fig. 11.

Notably, in the chaotic regions, the time between a maximum point and a minimum of point of $x_1(t, 0, 0, b)$ is approximately $T/2$. Tracing the maximum and minimum points of the x_1-coordinates of ω_b, yields an approximate Poincaré $T/2$-map,

$$\hat{F}(\xi_1, \xi_2) \equiv \left(x_1\left(\frac{T}{2}; \xi_1, \xi_2\right), \quad x_2\left(\frac{T}{2}; \xi_1, \xi_2\right)\right), \tag{78}$$

which is double the Poincaré T-map F given in (9).

7.2. *Impacts of the input periods*

This subsection briefly discusses the effects of the input period. Section 6, for a given T, discusses the types of asymptotic limit cycles Λ_∞ that arise as $b \to \infty$. Two different types arise according to separability. Λ_b and $-\Lambda_b$ is separable if $-\Lambda_b \neq \Lambda_b$ and separated by x_1-axis, which is ensured when T is relatively small. See Theorem 6.1. Otherwise, Λ_b and $-\Lambda_b$ are inseparable.

The numerical evidence indicates that separability is importantly involved in the occurrence of chaotic attractors. Apparently, separable Λ_b and $-\Lambda_b$ cause crises as b decreases to a particular threshold, for example, near b_3^* in the ZN-case.

In the search for chaotic regions, Theorem 6.1 is first applied to $T \leq T_0^*$ as in (67). For those T, b near $b^*(T) = T_0(A)/T$ is first tried. Computing three critical trajectories at b_1^*, b_2^* and b_3^* is important. Normally, b_1^*, b_2^* and b_3^* near $b^*(T)$ whenever they exist. In the ZN-case, the graphs of b^*, b_1^*, b_2^* and b_3^* are drawn and compared with the regions in which (1) has a positive Lyapunov exponent (≥ 0.02). See Fig. 19. Notably, the chaotic regions of (1) are marked by $\circ$ in Fig. 19. Since the chaotic regions and windows regions interweave each other, the marker $\circ$ in Fig. 19 is necessarily isolated for each T.

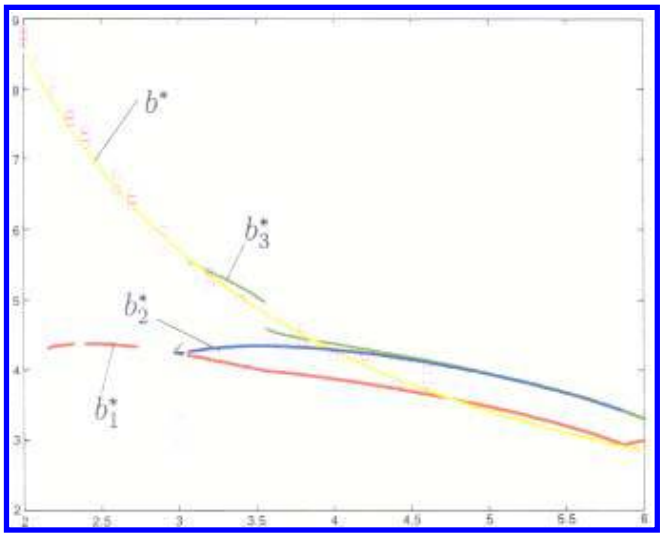

Fig. 19. Critical numbers b^*, b_k^*, $k = 1, 2, 3$ for varying T, $A = [1.2, 2, -1.2]$.

The computed results are stated as follows.

Theorem 7.1. *Given a template* $A = [r, p, s]$ *that satisfies* (*3*), (*1*) *has a chaotic region on* $[b_1^*(T), b_3^*(T)]$ *provided the input period* T *satisfies* (*67*) *and* $b_1^*(T)$, $b_2^*(T)$ *and* $b_3^*(T)$ *exist.*

Notably, critical trajectories $\Gamma_b(0, 0)$ that circle around O ℓ-times, C^+ m-times and C^- n-times at critical numbers $b_{\ell,m,n}^*$ can be induced. See Figs. 19 and 20 for $T = 2$ or $T = 3$. In that case, analogue results similar to Theorem 7.1 can be stated. The details are omitted here.

For $T \in [3.5, 4.5]$, chaotic phenomena similar to $T = 4$ were observed. For $T \geq 5$, no chaotic regions are found. For $T \in [2, 3]$, chaotic regions exist but $\hat{\omega}_b$ are not a lady's shoe. See Figs. 20(a)–20(h).

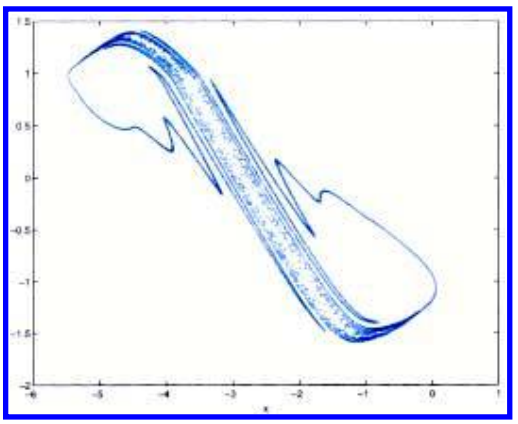

(a) $T = 2$ and $b = 8.88$

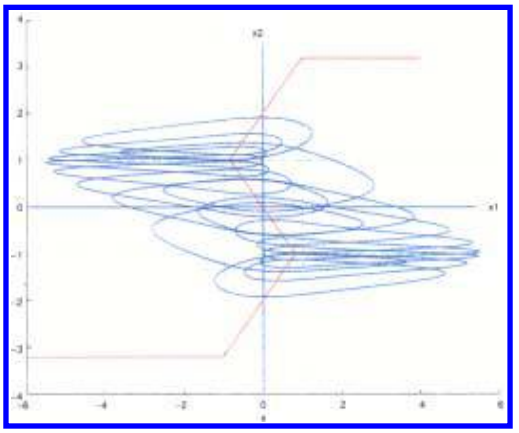

(b) $T = 2$ and $b = 8.872$

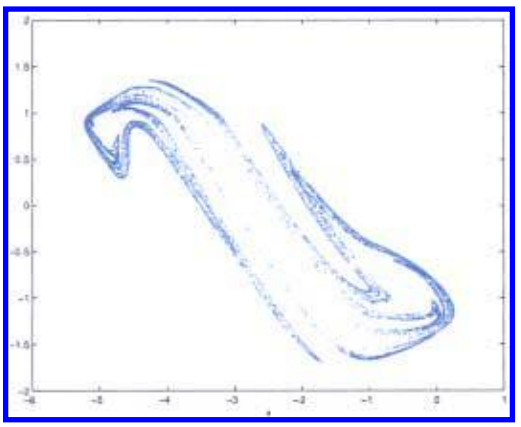

(c) $T = 3$ and $b = 5.844$

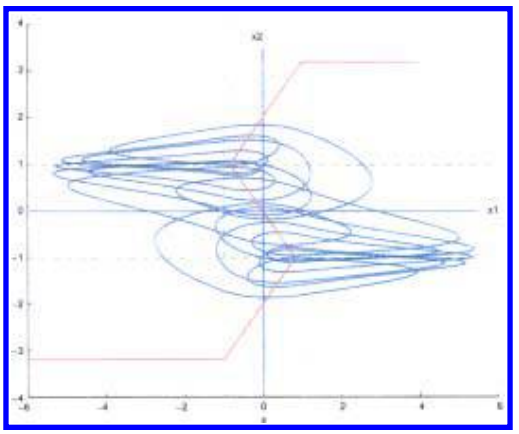

(d) $T = 3$ and $b = 5.828$

Fig. 20. Chaotic attractors and basic periodic cycles for $A = [1.2, 2, -1.2]$ with varying T.

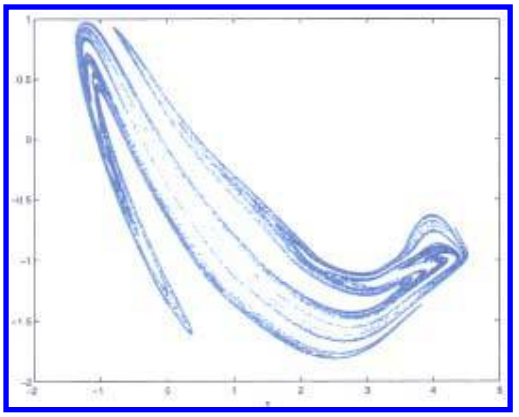

(e) $T = 3.5$ and $b = 4.94$

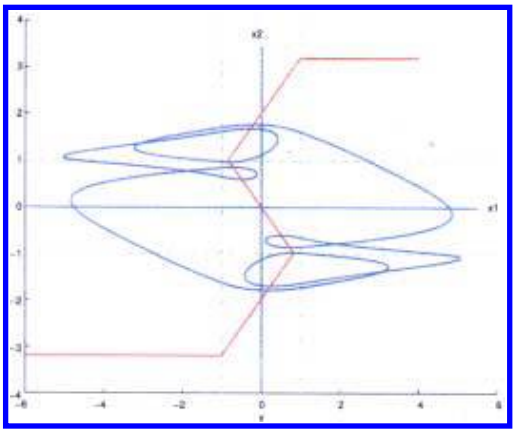

(f) $T = 3.5$ and $b = 4.901$

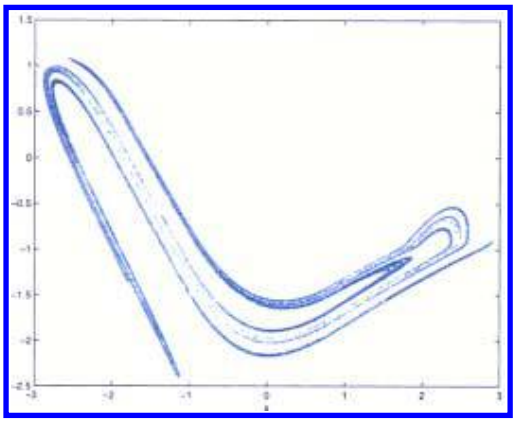

(g) $T = 4.5$ and $b = 3.86$

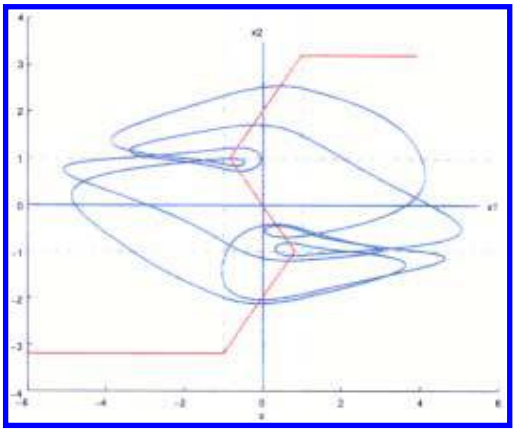

(h) $T = 4.5$ and $b = 3.822$

Fig. 20. (*Continued*)

7.3. *Varying templates*

The role of template $A = [r, p, s]$ is fundamental. It governs the basic dynamics among the inputs. A more complete study of the effects of the template is required. Some preliminary results are presented here; very interesting results can be obtained by varying the templates.

Since the first criterion that determines whether ω_b is a chaotic attractor is that ω_b must has a positive Lyapunov exponent, let $\lambda_1(b, T, r, p, s)$ be the largest Lyapunov exponent of $\omega(b, T, r, p, s)$ and define

$$\lambda_1^*(r, p, s) = \sup_{b>0, T>0} \lambda_1(b, T, r, p, s)\,. \tag{79}$$

Then, the template $A = [r, p, s]$ can introduce a chaotic attractor with a suitable input $bu(t)$ if $\lambda_1^*(r, p, s) > 0$. Instead of considering all $b > 0$ and $T > 0$ in (79), denote

$$\lambda^*(r, p, s) = \max\{\lambda_1(b, T, r, p, s)| \tag{80}$$

$$\delta T_0^* \le T \le T_0^* \text{ and } \delta_1 b^*(T) \le b \le \delta_2 b^*(T)\}\,,$$

where T_0^* is defined in (67) and $b^*(T)$ is defined in (31), δ and δ_1 are small positive numbers, for example $\delta = \delta_1 = 0.1$, and $\delta_2 = 2$. Numerical evidence suggests that $\lambda^*(r, p, s)$ closely approximates to $\lambda_1^*(r, p, s)$.

Antisymmetric A is first considered, i.e. $s = -r$, and write

$$\lambda^*(r, p) = \lambda^*(r, p, -r)\,. \tag{81}$$

Taking $p = 2$ in (81), the graph of $\lambda^*(r, 2)$ is plotted for $r \in (1, 6)$. See Fig. 21. Notably, in the ZN-case, i.e. $r = 1.2$ is not a maximum point for $\lambda^*(r, 2)$. Indeed, when most r are in [3, 4.5], a higher Lyapunov exponent exists, and can induce more complex chaotic behaviors. See Fig. 23(c).

Some preliminary results are also obtained for asymmetric templates. See Fig. 23. For asymmetric templates, $\lambda^*(r, 2, s)$ are computed over some ranges. See Fig. 22. The marker $\odot$ indicates for

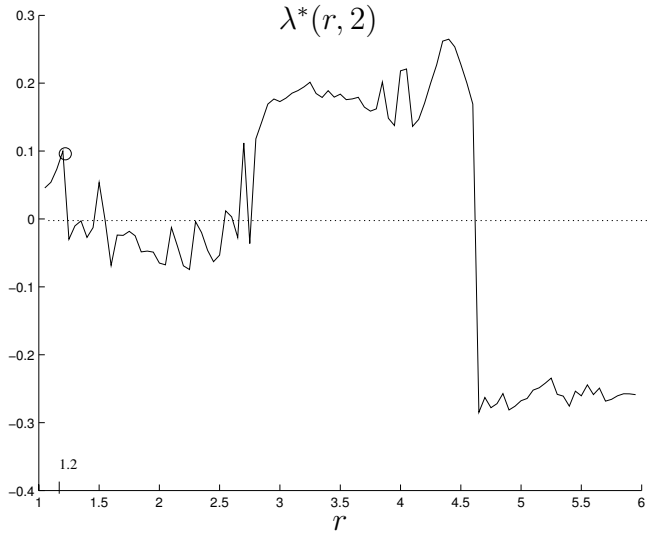

Fig. 21. The maximum Lyapunov exponent function $\lambda^*(r, 2)$ for $A = [r, 2, -r]$.

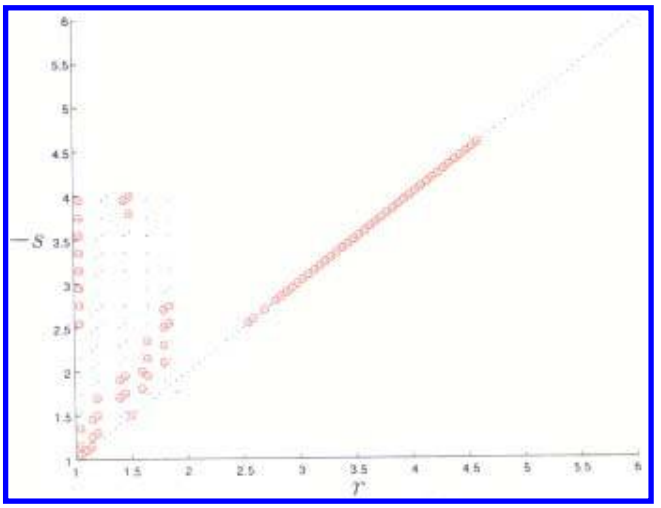

Fig. 22. The maximum Lyapunov exponent for $\lambda^*(r, 2, s)$ maker $\odot$ for $\lambda^* > 0$ and $\cdot$ for $\lambda^* < 0$.

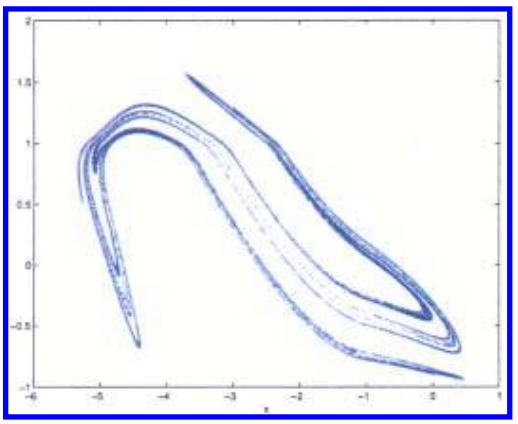

(a) $A = [1.2, 2, -1.3]$, $b = 4.16$, $T = 4.3$

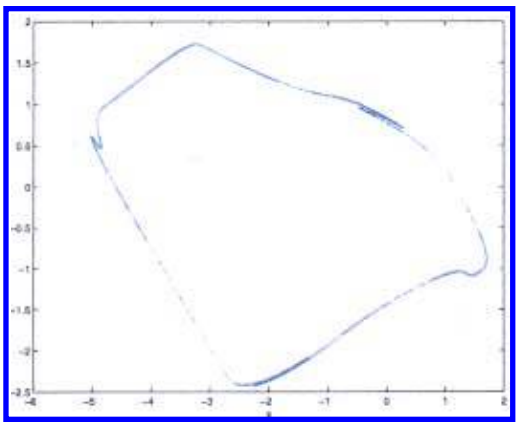

(b) $A = [1.5, 2, -1.7]$, $b = 4.7$, $T = 2.62$

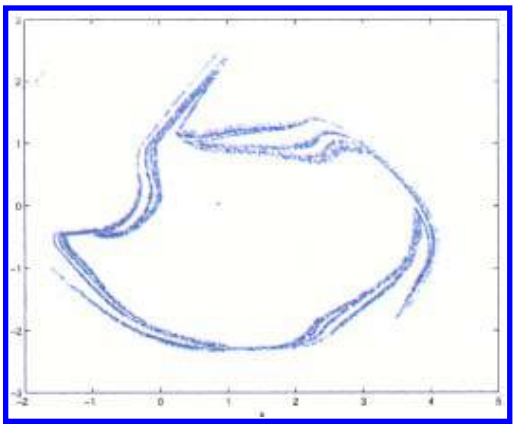

(c) $A = [4.5, 2, -4.5]$, $b = 6.9883$, $T = 1.31$

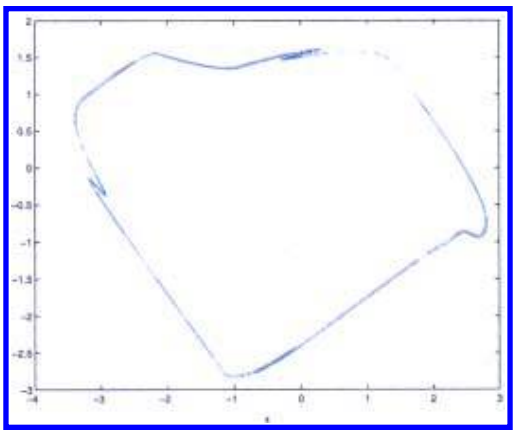

(d) $A = [1.5, 2, -1.75]$, $b = 4.28$, $T = 2.08$

Fig. 23. Some typical chaotic attractors for general $A = [r, 2, s]$.

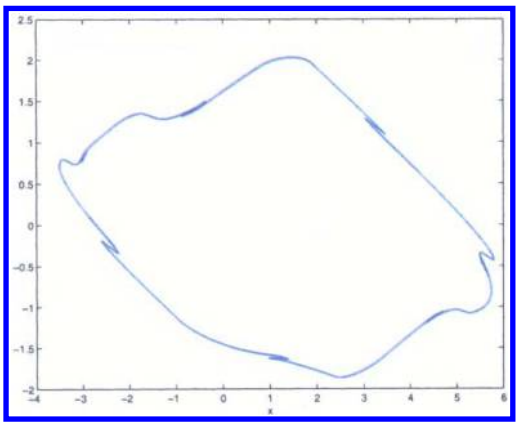

(e) $A = [1.5, 2, -4]$, $b = 9.06$, $T = 0.88$

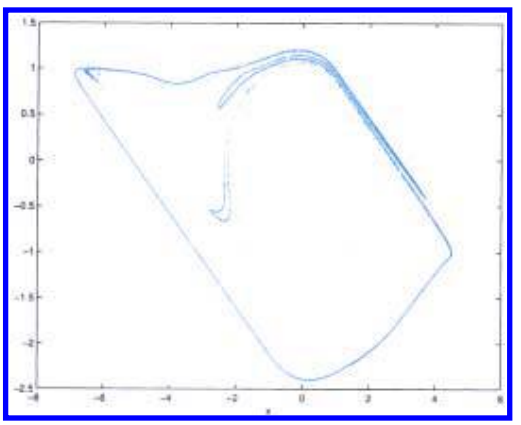

(f) $A = [1.05, 2, -3.95]$, $b = 2.72$, $T = 6.2$

Fig. 23. (*Continued*)

those $A = [r, 2, s]$ for which $\lambda^*(r, 2, s)$ is positive and $\cdot$ is nonpositive. Figure 23 plots some typical chaotic attractors for antisymmetric and general asymmetric templates. Notably, most are not lady's shoes. The more detailed results concerning bifurcations and chaos will be reported elsewhere.

8. Numerical Methods

This section describes the several numerical methods used herein, including the Poincaré map, the FFT and the Lyapunov exponent.

The trajectory of the system (1) must first be generated. Numerically, for a given set of parameters, a template $A = [r, p, s]$ that satisfies (3), an amplitude b and period T, the system of differential equations is solved in FORTRAN 90 by calling a subroutine, RKF45, using the Runge–Kutta–Fehlberg (4, 5) methods described in [Fehlberg, 1968], with step size = 0.05, absolute error 1×10^{-10} and relative error 1×10^{-8}.

Since the ω-limit set $\omega(b, T, A)$ is of greatest concern, 2×10^6 steps are taken in the RKF45 integration. The first 1×10^6 steps were ignored, and the following numerical methods applied to the remaining data; the last 1×10^6 points were taken as the ω-limit set $\omega(b, T, A)$.

The ω-limit set $\hat{\omega}(b, T, A)$ of Poincaré T-map is taken every T/stepsize points from $\omega(b, T, A)$. The relative error of the Poincaré map can be easily computed. For example, in the ZN-case $T = 4$ with a step size 0.05, 80 steps must be integrated for each point on the Poincarè map. Therefore, the relative error $1 \times 10^{-8} \times 80 = 8 \times 10^{-7}$ is obtained for each successive point of the Poincaré map.

The Lyapunov exponents are obtained by averaging eigenvalues of $DF(\xi_1, \xi_2)$ on each point in $\hat{\omega}_b$. Here, a convergent condition is imposed that the relative error is less than 1×10^{-4}. Moreover, the first 1×10^6 steps in the numerical integration are ignored to accelerate the convergence.

9. Conclusions

Zou and Nossek [1991] discovered a chaotic attractor in a two-cell CNN with template $A = [1.2, 2, -1.2]$ and input $b \sin(2\pi/T)$ with $T = 4$ and $b \cong 4.08$. This work investigates bifurcations and chaos for a broad range of templates $A = [r, p, s]$, input period $T > 0$ and input amplitude $b > 0$.

The bifurcations of (1) involve five parameters; r, p, s, T and b. The strategy used herein is to begin with $b = 0$ and A satisfying (3). Section 4 studied the existence and multiplicity problems of periodic cycle of (1). The existence of the limit cycle $\Lambda_0(A)$ is proven when (3) holds. The existence and multiplicity of exterior periodic cycles are studied under further assumptions. The uniqueness problem is still open for general A that satisfies (3). The numerical evidence suggests that the limit cycle is unique.

The bifurcation problem is studied by examining how "typical" trajectories vary with b, T and A. In particular, the trajectory $\Gamma(b, T, A)$ and its ω-limit set $\omega(b, T, A)$ with initial conditions at the origin $O = (0, 0)$, are considered. The system (1) is considered to be chaotic, if

(i) $\Gamma(b, T, A)$ has a positive Lyapunov exponent,
(ii) The Poincaré T-map $\hat{\omega}(b, T, A)$ of $\omega(b, T, A)$ is fractal and

(iii) FFT of $\Gamma(b, T, A)$ has a broad-band.

Section 6 presented an approach to study the effects of the input T by examining the asymptotic limit cycle $\Lambda_\infty(T, A)$ with period T of $\Gamma(b, T, A)$ as $b \to \infty$. When $T \le T_0^*$, as defined in (67), then $\Lambda\infty$ and $-\Lambda_\infty$ can be separated. Therefore, $\omega(b, T, A)$ and $-\omega(b, T, A)$ are separated for large b and may collide when b is small. If b becomes even smaller then a chaotic attractor may develop. The onset of chaos induced by crises $\omega(b, T, A)$ and $-\omega(b, T, A)$ was observed for suitable T and b. These cases includes the ZN-case, $A = [1.2, 2, -1.2]$ and $T = 4$. However, (67) alone does not cause chaos.

Section 3 presented a heuristic argument to determine the range of b over which maximum variation of $\Gamma(b, T, A)$ may occur. $b^*(T) = c_0 T_0(A)/T$ is introduced in (31) where $c_0 = c_0(A, T)$ and $c_0 = 1$ is a good estimate for practical purposes. In most cases, the chaotic regions occur with $c_0 \in [0.8, 1]$.

After a range of interest of T and b are identified, the effect of b can be studied. The primary mean is to compare the relative strengths of sustained limit cycle $\Lambda_0(A)$ (without input) and the input $bu(t)$.

The FFT of $\Gamma(b, T, A)$ is now obtained and the ratio $\mathcal{A}(b) \equiv |a_T(b)|/|a_1(b)|$, given in (10) of the largest amplitude $a_1(b)$ except for T-mode to the amplitude $a_T(b)$ of the periodic T-mode is considered. Section 5 considers $\mathcal{A}(b) \ll 1$, i.e. $\Lambda_0(A)$ dominates. $\omega(b, T, A)$ is found to be either quasi-periodic or periodic. Conjecture 5.1, which was partially proven, stated that periodic windows form a devil's staircase when $b \in (b_*, b_0^*)$ where $0 < b_* < b_0^*$. The conjecture will be proven if some continuity and transversality conditions are met for the two-dimensional Poincaré map $F(\xi_1, \xi_2)$ at periodic points. A well-known example of the devil's staircase is the bifurcations of one-dimensional logistic map $F_\lambda(x) = \lambda x(1 - x)$, $\lambda \in [1, 4]$, where periodic windows form a devil's staircase.

Section 7 examins the chaos by studying the effects of b, T and A in three subsections. When $\mathcal{A}(b) \sim 1$, i.e. $b \sim b^*(T, A)$, the Lyapunov exponents of $\Gamma(b, T, A)$ and $\hat{\omega}(b, T, A)$ are computed. In many interesting cases, finitely many chaotic regions and window regions interweave with each other.

Section 7.1 studies in detail the ZN-case with varying b. Figure 18 plots typical chaotic attractors and basic periodic cycles. Different characteristics of $\omega(b, T, A)$ in windows are considered. In each window, a sequence of periodic-doubling is observed to the left of the basic periodic cycle. A quasi-periodic region is to the right of the basic periodic cycle. Several outstanding questions remain to be answered. For example,

(i) Is any fine structure present in the quasi-periodic region of the windows?
(ii) Can any ergodic measure exist in chaotic regions? How do they change with regions?
(iii) Does any specific relationship exist between the chaotic regions and their neighboring window regions?

Section 7.2 considers the effect of input period T. The chaotic attractors, including especially the shape of $\hat{\omega}(b, T, A)$, depend strongly on T. In the ZN-case, $A = [1.2, 2, -1.2]$, $\hat{\omega}(b, T, A)$ look like a lady's shoe for $T \in [3.5, 4.5]$. However, for T smaller, say $T \le 3$, the shape changes. See Fig. 20. Apparently, the horseshoe or the partial horseshoe is visible in all cases. A detailed study of the effect of input period T is being conducted.

Section 7.3 considers the fundamental role of the template A. Figures 22 and 23 present some preliminary and interesting results obtained by varying templates in the antisymmetric and asymmetric regions. Considering $p = 2$, the regions in $(r, -s)$ parameter space were investigated to locate where chaos can occur. The chaotic parameters and nonchaotic parameters are spread out. Chaotic parameters cluster in some specific places which are easily identified, for example, along the antisymmetric line, i.e. $r = -s$. It is of great interest to study these chaotic bifurcations.

Acknowledgments

The authors would like to thank Dr. Ban, Jung Chao for several interesting discussions during the preparation of this work.

References

Alligood, K. T., Sauer, T. D. & Yorke, J. A. [1997] *Chaos, an Introduction to Dynamical System* (Springer).

Ban, J. C., Chien, K. P., Hsu, C. H. & Lin, S. S. [2001a] "Spatial disorder of cellular neural networks — with asymmetric output function," *Int. J. Bifurcation and Chaos* **11**, 2085–2095.

Ban, J. C., Lin, S. S. & Shih, C. W. [2001b] "Exact number of mosaic patterns in cellular neural networks," *Int. J. Bifurcation and Chaos* **11**, 1645–1653.

Ban, J. C., Hsu, C. H. & Lin, S. S. [2002] "Spatial disorder of cellular neural networks — with biased term," *Int. J. Bifurcation and Chaos* **12**, 525–534.

Chua, L. O. & Yang, L. [1988a] "Cellular neural networks: Theory," *IEEE Trans. Circuits Syst.* **35**, 1257–1272.

Chua, L. O. & Yang, L. [1988b] "Cellular neural networks: Applications," *IEEE Trans. Circuits Syst.* **35**, 1273–1290.

Chua, L. O. & Roska, T. [1993] "The CNN paradigm," *IEEE Trans. Circuits Syst.* **40**, 147–156.

Chua, L. O. [1998] *CNN: A Paradigm for Complexity*, World Scientific Series on Nonlinear Science, Series A, Vol. 31.

Chua, L. O. & Roska, T. [2002] *Cellular Neural Networks and Visual Computing: Foundation and Applications* (Cambridge University Press).

Fehlberg, E. [1968] "Low-order classical Runge–Kutta formulas with stepsize control," NASA TR R–315.

Hsu, C. H., Juang, J., Lin, S. S. & Lin, W. W. [2000] "Cellular neural networks: Local patterns for general templates," *Int. J. Bifurcation and Chaos* **10**, 1645–1659.

Hsu, C. H. & Lin, S. S. [2001] "Spatial disorder of cellular neural networks," *Japan J. Industrial and Appl. Math.* **19**, 143–161.

Hsu, C. H. & Yang, T. H. [2002] "Abundancce of mosaic patterns for CNN with spatially variant templates," *Int. J. Bifurcation and Chaos* **12**, 1321–1332.

Juang, J. & Lin, S. S. [1997] "Cellular neural networks: defect pattern and spatial chaos," preprint.

Juang, J. & Lin, S. S. [2000] "Cellular neural networks: mosaic pattern and spatial chaos," *SIAM J. Appl. Math.* **60**, 891–915.

Lin, S. S. & Shih, C. W. [1999] "Complete stability for standard cellular neural networks," *Int. J. Bifurcation and Chaos* **9**, 909–918.

Lin, S. S. & Yang, T. S. [2000] "Spatial entropy of one dimensional celluar neural network," *Int. J. Bifurcation and Chaos* **10**, 2129–2140.

Lin, S. S. & Yang, T. S. [2002] "On the spatial entropy and patterns of two-dimensional cellular neural network," *Int. J. Bifurcation and Chaos* **12**, 115–128.

Manganaro, G., Arena, P. & Fortuna, L. [1999] *Cellular Neural Networks: Chaos, Complexity, and VLSI Processing* (Springer).

Parker, T. S. & Chua, L. O. [1989] *Practical Numerical Algorithms for Chaotic Systems* (Springer-Verlag).

Perko, L. [1996] *Differential Equations and Dynamical Systems* (Springer).

Shih, C. W. [2001] "Complete stability for a class of cellular neural networks," *Int. J. Bifurcation and Chaos* **11**, 169–177.

Thiran, P. [1993] "Influence of boundary conditions on the behavior of cellular neural networks," *IEEE Trans. Circuits Syst.-I: Fund. Th. Appl.* **40**, 207–212.

Thiran, P., Crounse, K. R., Chua, L. O. & Hasler, M. [1995] "Pattern formation properties of autonomous cellular neural networks," *IEEE Trans. Circuits Syst.* **42**, 757–774.

Thiran, P. [1997] *Dynamics and Self-Organization of Locally Coupled Neural Networks* (Press Polytechniques et Universitaires Romandes, Lausanne, Switzerland).

Wu, C. W. & Chua, L. O. [1997] "A more rigorous proof of complete stability of cellular neural networks," *IEEE Trans. Circuits Syst.-I* **44**, 370–371.

Zou, F. & Nossek, J. A. [1991] "A chaotic attractor with cellular neural networks," *IEEE Trans. Circuits Syst.* **38**, 811–812.

Zou, F., Katérle, A. & Nossek, J. A. [1993] "Homoclinic and heteroclinic orbits of the three cells cellular neural networks," *IEEE Trans. Circuits Syst.* **40**, 843–848.

Zou, F. & Nossek, J. A. [1993] "Bifurcation and chaos in cellular neural networks," *IEEE Trans. Circuits Syst.* **40**, 166–173.